

F1: A VISION-LANGUAGE-ACTION MODEL BRIDGING UNDERSTANDING AND GENERATION TO ACTIONS

Qi Lv^{1,2,*}, Weijie Kong^{1,*}, Hao Li^{1,2,*}, Jia Zeng^{1,†}, Zherui Qiu¹, Delin Qu¹, Haoming Song¹, Qizhi Chen¹, Xiang Deng², Jiangmiao Pang^{1,†}


¹Shanghai AI Laboratory ²Harbin Institute of Technology (Shenzhen)

*Equal Contributions, †Corresponding Authors

{zengjia, pangjiangmiao}@pjlab.org.cn

 **Homepage:** <https://aopolin-lv.github.io/F1-VLA>

 **Github:** <https://github.com/InternRobotics/F1-VLA>

 **Huggingface:** <https://huggingface.co/InternRobotics/F1-VLA>

ABSTRACT

Executing language-conditioned tasks in dynamic visual environments remains a central challenge in embodied AI. Existing Vision-Language-Action (VLA) models predominantly adopt reactive state-to-action mappings, often leading to short-sighted behaviors and poor robustness in dynamic scenes. In this paper, we introduce \mathcal{F}_1 , a pretrained VLA framework which integrates the *visual foresight generation* into decision-making pipeline. \mathcal{F}_1 adopts a Mixture-of-Transformer architecture with dedicated modules for perception, foresight generation, and control, thereby bridging understanding, generation, and actions. At its core, \mathcal{F}_1 employs a next-scale prediction mechanism to synthesize goal-conditioned visual foresight as explicit planning targets. By forecasting plausible future visual states, \mathcal{F}_1 reformulates action generation as a foresight-guided inverse dynamics problem, enabling actions that implicitly achieve visual goals. To endow \mathcal{F}_1 with robust and generalizable capabilities, we propose a three-stage training recipe on an extensive dataset comprising over 330k trajectories across 136 diverse tasks. This training scheme enhances modular reasoning and equips the model with transferable visual foresight, which is critical for complex and dynamic environments. Extensive evaluations on real-world tasks and simulation benchmarks demonstrate \mathcal{F}_1 consistently outperforms existing approaches, achieving substantial gains in both task success rate and generalization ability.

1 INTRODUCTION

Vision-Language-Action (VLA) models (Kim et al., 2024; Team et al., 2025a; Black et al., 2024) aim to equip robots with the ability to execute natural language instructions in visually rich environments. By aligning language instructions with perceptual inputs and mapping them to actions, such models enable language-guide manipulation and versatile human-robot interaction. However, reliable performance in realistic settings remains elusive: environments are inherently dynamic, i.e., objects move, contexts shift, and instructions unfold over time, so robots must ground ambiguous language, handle diverse objects, and maintain long-horizon temporal coherence as scenes evolve. These conditions expose a core limitation of purely reactive state-to-action mappings: without predictive foresight about likely future states, policies become short-sighted and brittle under distribution shifts.

Previous efforts on manipulation policy learning can be broadly grouped into three paradigms, as illustrated in Fig. 1. The earliest line of work employs only an *action expert* trained end-to-end from observations to low-level actions (Zhao et al., 2023; Chi et al., 2023), but such purely reactive mappings lack semantic grounding and generalization across tasks and embodiments (Fig. 1(a)). To overcome these limitations, subsequent approaches integrate Vision-Language-Models (VLMs)

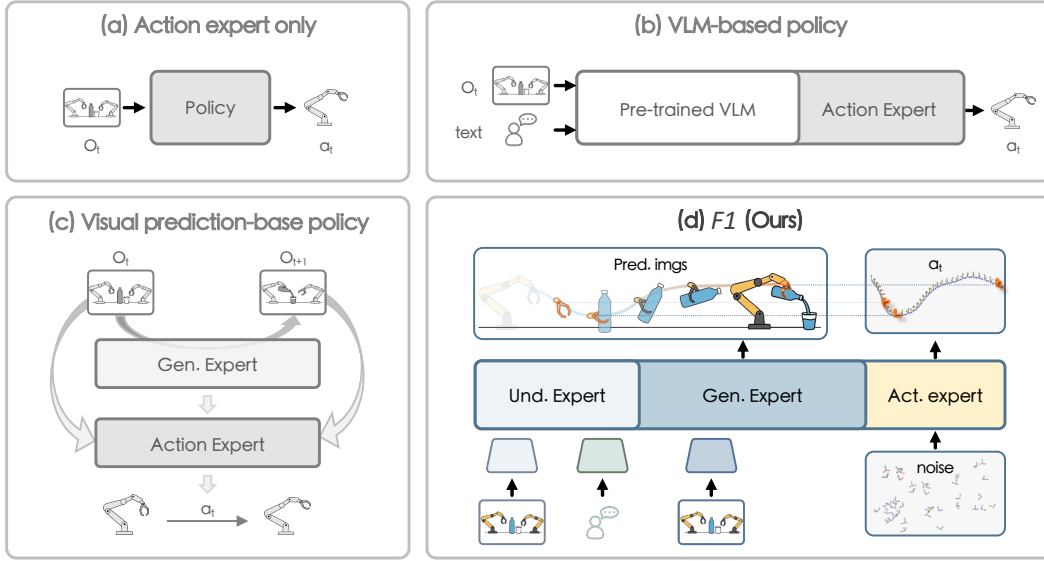


Figure 1: **The comparison of varied paradigms for manipulation policies.** The earliest end-to-end manipulation policies are illustrated in Fig. 1(a), such as ACT (Zhao et al., 2023) and DP (Chi et al., 2023). Policies shown in Fig. 1(b) introduce VLM, aiming to empower the action expert with the general capabilities of VLM in scene and instruction understanding, like π_0 (Black et al., 2024) and gr00t-N1 (Bjorck et al., 2025). There are also approaches, as seen in Fig. 1(c), e.g., VPP (Hu et al., 2024) and Genie Envisioner (Liao et al., 2025b), that leverage video diffusion models to guide action execution through video prediction. As depicted in Fig. 1(d), we adopt an integrated architecture of understanding, generation, and execution, empowering the action execution module with capabilities in both scene and instruction comprehension as well as dynamic temporal prediction.

into the policy, leveraging pretrained multimodal knowledge to enhance scene and instruction understanding (Black et al., 2024; Bjorck et al., 2025) (Fig. 1(b)). However, they lack temporal evolutionary modeling and remain reactive in nature, thus failing to cope reliably with dynamic or long-horizon manipulation tasks. More recently, visual prediction-based policies (Hu et al., 2024; Liao et al., 2025b) attempt to anticipate future observations as auxiliary signals (Fig. 1(c)), but without integrating semantic understanding from VLMs, their predictions lack semantic grounding and result in brittle control, offering limited robustness and generalization.

Across these paradigms, the main limitation is their reliance on reactive state-to-action mappings, which leads to short-sighted behavior and fragility under dynamic and complex manipulation tasks. This motivates a central question: ***What architectural and training principles are required to move beyond reactive imitation and toward robust, foresight-driven policy?***

Inspired by the Predictive Inverse Dynamics Models (Tian et al., 2024c; Black et al., 2023; Du et al., 2023), we introduce \mathcal{F}_1 , a VLA framework that integrates goal-conditioned visual foresight into the perception-action loop (Fig. 1d). PIDMs predict a future state first, and then frame control as inferring the actions required to realize a desired future observation. By adopting this principle, \mathcal{F}_1 reformulates action generation as foresight-guided inverse dynamics: actions are derived not only from the current observation, but also from an anticipated visual outcome. Specifically, \mathcal{F}_1 adopts a Mixture-of-Transformer (MoT) (Liang et al., 2025) architecture with three dedicated experts for understanding, foresight generation, and action execution, thereby bridging perception, prediction, and control in a unified framework. To equip the model with robust and transferable capabilities, we design a progressive three-stage training recipe.

From the perspective of model architecture, \mathcal{F}_1 introduces two key designs. First, a progressive attention scheme regulates information exchange across experts: intra-expert attention captures rich token interactions, while inter-expert attention enforces a causal flow from understanding to foresight to action, ensuring stability and interpretability. Second, the generation expert employs a next-scale prediction mechanism (Tian et al., 2024b) to synthesize goal-conditioned visual foresight

efficiently, producing explicit planning targets that guide subsequent control. These designs enable \mathcal{F}_1 to explicitly couple semantic understanding, predictive foresight, and action execution within a unified backbone.

From the perspective of training strategy, we propose a three-stage recipe that progressively aligns and integrates the experts. Stage I injects foresight capability by aligning the generation expert with the understanding expert which inherits from a pretrained MLLM. Stage II pretrains the entire model on large-scale public robot datasets to learn general shared visuomotor knowledge. Stage III post-trains on task-specific data to adapt the model to new embodiments and fine-grained manipulation skills. This progressive scheme not only stabilizes optimization but also endows the model with generalizable foresight, which is critical for robustness in dynamic and long-horizon tasks.

Overall, we present \mathcal{F}_1 , a pretrained Vision-Language-Action model with 4.2B parameters. Building on predictive inverse dynamics modeling, \mathcal{F}_1 introduces visual foresight as an explicit planning signal and couples it with action generation through a progressive training scheme. Extensive experiments in both real-world and simulation benchmarks demonstrate that \mathcal{F}_1 substantially improves success rates and robustness compared to reactive baselines, particularly in dynamic and long-horizon tasks. In summary, our contributions are as follows:

- We introduce a novel paradigm for VLA models by integrating a dedicated generation expert that leverages a predictive inverse dynamics model to forecast visual observation, fundamentally transforming action prediction from a reactive to a planning-based process.
- To ensure robustness and generalizability, we develop a three-stage training recipe. This carefully designed scheme progressively integrates the model’s distinct understanding, generation, and action modules.
- Our model \mathcal{F}_1 demonstrates superiority in both simulation and real-world tasks. We show substantial improvements over reactive baselines, particularly in challenging dynamic environments and long-horizon tasks that require robust planning and foresight.

2 THE \mathcal{F}_1 FRAMEWORK: BRIDGING PERCEPTION, FORESIGHT, TO ACTIONS

We present \mathcal{F}_1 , a Vision-Language-Action (VLA) model that bridges perception, visual foresight generation, to action execution through a Mixture-of-Transformer (MoT) architecture (Liang et al., 2025). By jointly modeling understanding, foresight, and control, \mathcal{F}_1 enables language-conditioned agents to plan and act robustly in complex environments.

2.1 ARCHITECTURE OVERVIEW

As illustrated in Fig. 2, \mathcal{F}_1 comprises three dedicated experts: **an understanding expert, a generation expert, and an action expert**. Given an instruction l and current observation o_t , the understanding expert encodes semantic and visual information to establish a shared multimodal representation. This representation is then passed to the foresight generation expert, which predicts a goal-conditioned visual foresight \hat{o}_{t+1} . To capture temporal dynamics, the foresight module additionally leverages a sequence of past observations $\{o_{t-m}, \dots, o_{t-1}\}$, thereby grounding the prediction in both historical context and task goals. Finally, the predicted foresight image \hat{o}_{t+1} is fed into the action expert, which formulates a predictive inverse dynamics modeling problem, enabling the model to generate an action chunk $\hat{a}_{t:t+k}$ that drives the robot toward the synthesized visual target.

2.2 UNIFIED UNDERSTANDING-GENERATION-ACTION TRANSFORMER

Building on the demonstrated effectiveness of decoder-only transformers across large models (OpenAI et al., 2024; Yang et al., 2025a; Bai et al., 2025; Liu et al., 2023b), \mathcal{F}_1 instantiates all three experts with a common decoder-only architectural backbone, enabling scalable autoregressive modeling while retaining expert-specific specialization.

Understanding Expert. To achieve robust alignment between natural language instructions and perceptual inputs, the understanding expert is initialized from a pretrained vision-language model trained on large-scale paired text-image data. At each timestep, the current visual observation o_t is first encoded by a SigLIP vision encoder (Zhai et al., 2023) to produce high-level perceptual features.

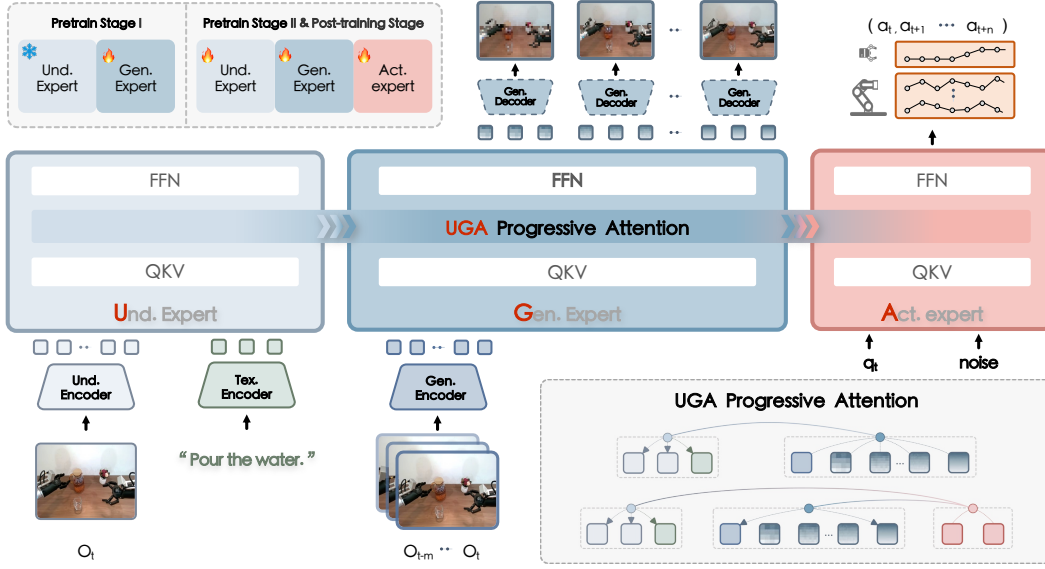


Figure 2: **Overview of \mathcal{F}_1 framework.** It employs the Mixture-of-Transformer (Liang et al., 2025) architecture comprising three core components: an understanding expert, a generation expert, and an action expert. The understanding expert processes instructions and observations to generate a foresight image. The visual foresight is then fed to action expert to predict a target action via the predictive inverse dynamics modeling (Tian et al., 2024c; Du et al., 2023).

These features are fused with the language prompt and processed by the decoder-only transformer, allowing the expert to capture semantic correspondences between task goals and the observed scene. This design equips the understanding expert with reliable, semantically aligned representations that serve as the foundation for subsequent foresight generation and action execution.

Generation Expert. The generation expert is designed to produce a foresight image \hat{o}_{t+1} conditioned on the current observation o_t and the language goal l , serving as an explicit intermediate target for subsequent control. In contrast to conventional reactive policies, this module anticipates plausible future visual states, thereby enabling smoother and more adaptive behaviors in dynamic environments. Efficient foresight prediction is challenging, since high-fidelity visual synthesis often incurs substantial computational cost. To mitigate this issue, we employ a next-scale prediction strategy that balances computational efficiency with predictive accuracy.

Concretely, recent observations $\{o_{t-m}, \dots, o_t\}$ are first encoded by a multi-scale residual vector quantization (VQ) encoder (Lee et al., 2022). As illustrated in Fig. 3, each frame is decomposed into 16×16 patches across k spatial scales $\{r_1, \dots, r_k\}$, yielding discrete tokens $\{z_i^0, \dots, z_i^k\}$ for each o_i . To avoid prohibitively long sequences from concatenating tokens across multiple frames, a temporal convolutional network aggregates motion-relevant features into a compact representation. This representation is then processed by a decoder-only transformer to autoregressively generate foresight tokens, which are subsequently decoded into the predicted future image \hat{o}_{t+1} . Through this design, the generation expert realizes an efficient mechanism for real-time foresight, supplying explicit visual targets that guide the inverse dynamics model in action execution.

Action Expert. The action expert is responsible for mapping the multimodal context into executable robot actions. Conditioned on the language goal l , the current observation o_t , and the generated foresight image \hat{o}_{t+1} , it predicts a short-horizon action sequence $\hat{a}_{t:t+k}$. By incorporating foresight

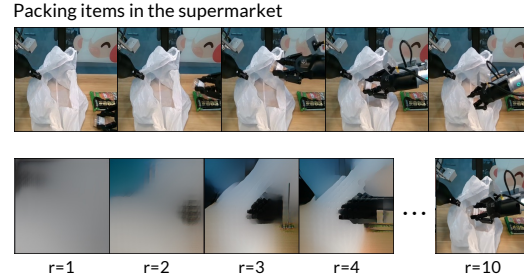


Figure 3: Visualization of Residual VQ-VAE from 16×16 to 256×256 resolution.

explicitly, the policy grounds its decisions not only in the present state but also in an anticipated visual target, which supports goal-directed and temporally consistent behavior. In practice, we employ a chunked action prediction (Zhao et al., 2023) which captures motion patterns over multiple steps and a flow-matching objective in continuous action space. Through this formulation, the action expert produces accurate and coherent action plans that are responsive to immediate observations while remaining consistent with long-term task objectives.

Attention Mechanism. To coordinate these heterogeneous experts, we introduce a hierarchical scheme termed *Understanding–Generation–Action (UGA) progressive attention*. Within each expert, bidirectional intra-expert attention enables comprehensive token interactions, except in the generation expert, where foresight tokens follow a causal, scale-conditioned pattern to preserve autoregressive consistency. Across experts, inter-expert attention follows a causal hierarchy: the generation expert attends to the understanding expert, while the action expert attends to both, but no information flows in the reverse direction. This progressive design enforces foresight as an explicit intermediate representation—preventing information leakage from actions back into foresight—thereby stabilizing training, enhancing interpretability, and ensuring that downstream control is genuinely guided by predicted visual outcomes rather than by shortcut correlations.

2.3 TRAINING RECIPE

We train \mathcal{F}_1 on a mixture of open-source datasets and task-specific collections, covering more than 320k trajectories across 136 tasks and 5 embodiments. Comprehensive statistics of the training corpus are provided in the Appendix A. Our training recipe follows a three-stage paradigm designed to progressively build alignment, generalization, and task adaptation: (i) **Pretrain Stage I**, aligning the generation expert with the understanding expert, (ii) **Pretrain Stage II**, pretraining the full model on large-scale public robot datasets, and (iii) **Post-train Stage**, post-training on task-specific demonstrations for embodiment adaptation.

Pretrain Stage I. The understanding expert inherits the weight from π_0 (Black et al., 2024), while the generation expert is randomly initialized. We then train the generation expert to synthesize future visual tokens conditioned on historical observations and language instructions, with outputs aligned to the semantic space established by the pretrained understanding expert. This stage injects generative foresight into the model while retaining the pretrained vision–language alignment.

Formally, given a sequence of historical observations $\{o_{t-m}, \dots, o_t\}$ and an instruction l , the generation expert predicts a foresight image \hat{o}_{t+1} whose VQ token representation is matched to the target. The training objective minimizes the negative log-likelihood of the ground-truth tokens:

$$\mathcal{L}_{\text{gen}}^{\text{gt}} = -\mathbb{E}_{\{o_i, l\} \sim \mathcal{D}} \left[\sum_{j=1}^N \log p_{\theta}(z_j \mid z_{1:j-1}^{\text{gt}}, \{o_i\}_{i=t-m}^t, l) \right], \quad (1)$$

where $z_j^{\text{gt}} = E(o_{t+1})_j$ are discrete tokens encoded by the residual VQ-VAE. We apply teacher forcing to stabilize autoregressive training at this stage.

Pretrain Stage II & Post-train Stage. After Stage I aligns the generation and understanding experts, we jointly optimize all three experts under a unified framework. There are two steps: Stage II pretrains the full model on large-scale public robot datasets for foundational visuomotor learning, and the post-train stage finetunes on task-specific demonstrations for embodiment adaptation. There are two objectives driving this process:

(1) *Autoregressive Next-Scale Prediction.* In contrast to the teacher-forcing regime in Stage I, we adopt an autoregressive formulation where each foresight token is generated conditioned on previously predicted tokens. Given historical observations $\{o_{t-m}, \dots, o_t\}$ and language instruction l , the model autoregressively generates future VQ tokens $\hat{z}_{1:N}$, where each prediction step conditions on previously generated tokens:

$$\mathcal{L}_{\text{gen}}^{\text{pred}} = -\mathbb{E}_{\{o_i, l\} \sim \mathcal{D}} \left[\sum_{j=1}^N \log p_{\theta}(z_j \mid \hat{z}_{1:j-1}, \{o_i\}_{i=t-m}^t, l) \right], \quad (2)$$

This autoregressive formulation enforces distributional consistency between training and inference, thereby enhancing generation stability and long-horizon coherence.

(2) *Flow Matching-based Action Prediction.* To establish a principled connection between foresight and motor control, we adopt flow matching (Lipman et al., 2023) to model the continuous transformation from Gaussian noise to expert actions. Given interpolated actions $a_t^\tau = (1 - \tau)\epsilon + \tau a_t$ with $\tau \sim \mathcal{U}(0, 1)$ and $\epsilon \sim \mathcal{N}(0, I)$, the policy π_θ learns vector fields that guide the transformation toward target actions:

$$\mathcal{L}_{\text{action}} = \mathbb{E}_{\{a_t, o_i, q_t, l\} \sim \mathcal{D}} \left[\left\| \pi_\theta(l, \{o_i\}_{i=t-m}^t, q_t, a_t^\tau) - (a_t - \epsilon) \right\|^2 \right], \quad (3)$$

where q_t denotes the proprioception information at time t .

The overall training objective is defined as a weighted sum of the two components:

$$\mathcal{L}_{\text{total}} = \mathcal{L}_{\text{gen}}^{\text{pred}} + \lambda \cdot \mathcal{L}_{\text{action}}, \quad (4)$$

with λ balancing the objectives. This joint optimization enforces representational consistency across experts, integrates foresight with control, and facilitates generalization over tasks and embodiments.

2.4 IMPLEMENTATION DETAILS

Model Architecture. \mathcal{F}_1 adopts a Mixture-of-Transformer architecture comprising an understanding expert, a generation expert, and an action expert. The architecture of understanding expert is implemented the same as PaliGemma (Beyer et al., 2024), while the generation and action experts follow the same Gemma backbone (Team et al., 2025b). The backbone integrates Swish activations (Ramachandran et al., 2017), RMSNorm normalization (Zhang & Sennrich, 2019), and Rotary Position Embeddings (Su et al., 2023). For initialization, the understanding and action experts are inherited from π_0 (Black et al., 2024), whereas the generation expert is randomly initialized and equipped with a pretrained residual VQ-VAE from VAR for image quantization (Tian et al., 2024a).

Dataset. \mathcal{F}_1 is trained on a large-scale corpus of robotic manipulation trajectories comprising approximately 330k episodes across 136 tasks. The corpus integrates widely used public benchmarks, including LIBERO (Liu et al., 2023a), Open-X-Embodiment (Collaboration et al., 2025), and Agi-BotWorld (AgiBot-World-Contributors et al., 2025) (see Appendix A for details). It spans a broad spectrum of skills, from elementary pick-and-place to complex behaviors such as grasping, handover, and pushing, and covers diverse temporal scales with episode lengths ranging from 10 seconds to over 2 minutes. This diversity in task complexity and temporal horizon provides rich supervision for developing robust visuomotor policies.

Training and Inference. Training proceeds in three sequential stages. In Pretrain Stage I, the understanding expert is frozen while the generation expert is trained with VAR to predict future images across 10 resolutions. In Stage II and the post-training stage, all experts are optimized jointly for end-to-end visuomotor learning. Further hyperparameter details, such as batch size and training steps, are provided in the Appendix B. For efficient real-time control during inference, foresight prediction is restricted to 4 scales.

3 EXPERIMENTS

To thoroughly evaluate our proposed \mathcal{F}_1 , we conduct extensive experiments across both simulated benchmarks and real-world tasks. Our evaluation not only validates the model’s core performance but also investigates its robustness and generalization in various challenging scenarios.

We first present a quantitative comparison of \mathcal{F}_1 with existing mainstream Vision-Language-Action models (Black et al., 2024; Kim et al., 2024; Bjorck et al., 2025) to demonstrate its superior performance. We then perform a series of comprehensive ablation studies to justify the necessity and contribution of each key component. Furthermore, to provide deeper insights into the model’s robustness, generalization, and rapid adaptation, we conduct several additional experiments. Specifically, we set up a kitchen environment with a conveyor belt to evaluate its performance on a challenging dynamic manipulation task involving a moving target. We also conduct experiments on various robot embodiments to evaluate the model’s ability to rapidly adapt to new platforms. Finally, we evaluate its long-term robustness in complex, sequential scenarios through a long-horizon task.



Figure 4: **Overview of real-world robot experiments.** We conduct 12 real-world robotic experiments on three different platforms: Genie-1, Franka, and ARX LIFT II. The experiments on Genie-1 are designed to evaluate the model’s ability to handle task diversity. The Franka experiments assess the model’s quick adaptation capabilities, while the ARX LIFT II tasks are used to benchmark its performance on challenging long-horizon manipulation problems.

3.1 COMPARISON ON THE REAL-WORLD TASKS

To further validate the performance of our proposed \mathcal{F}_1 , we conduct experiments on 9 real-world tasks using the Genie robot, a dual-arm manipulation platform as illustrated in Fig. 4. Details of the hardware platform and task setup are provided in Appendix C. For each task, we collect demonstrations and fine-tune \mathcal{F}_1 and baseline VLA models, including π_0 (Black et al., 2024), gr00t-N1 (Bjorck et al., 2025), and gr00t-N1.5 (Bjorck et al., 2025), for comparison. Each model is evaluated 15 times per task, and we report the average grasp and task success rates.

As shown in Tab. 1, \mathcal{F}_1 demonstrates superior performance across all tasks, achieving an average grasp rate of 92.6% and an average success rate of 82.2%. In contrast, the best-performing baseline, π_0 , only achieves 78.5% grasp and 65.2% success rates, while gr00t-N1 and gr00t-N1.5 perform even worse. These results clearly highlight the effectiveness of our foresight-guided design and modular reasoning capabilities. In terms of individual tasks, \mathcal{F}_1 achieves a perfect grasp rate (100%) on some tasks with correspondingly high success rates, e.g. *Pen*, *Flower*, *Chip*, and *Tea (Table)*. Notably, on more challenging tasks, i.e., *Handover (R2H)*, which require precise coordination and dynamic adjustment, \mathcal{F}_1 consistently outperforms baselines by large margins, achieving up to 93.3% success rate compared to π_0 (40%) and gr00t-N1 (13.3%). The superior performance of \mathcal{F}_1 can be attributed to its ability to predict plausible future visual states via next-scale prediction and leverage them as explicit planning targets. By transforming action generation into a foresight-guided inverse dynamics problem, \mathcal{F}_1 effectively bridges understanding, generation, and action, leading to improved robustness and generalization across diverse real-world tasks.

	Pen	Flower	Chip	Tea (Table)	Tea (Shelf)	Bread	Handover	Handover (R2H)	Mixture	Average
π_0	66.7%	66.7%	86.7%	86.7%	73.3%	66.7%	33.3%	40.0%	66.7%	65.2%
gr00t-N1	46.7%	33.3%	33.3%	40.0%	13.3%	33.3%	26.7%	13.3%	33.3%	30.4%
gr00t-N1.5	73.3%	40.0%	46.6%	73.5%	26.6%	53.3%	60.0%	40.0%	66.7%	53.3%
\mathcal{F}_1 (Ours)	93.3%	80.0%	100.0%	93.3%	86.7%	66.7%	80.0%	73.3%	66.7%	82.2%

Table 1: **Results on Real-world Tasks.** We test each model 15 times per task and report its average success ratio. The best results are denoted in **bold**. The experimental results show the superior performance of our \mathcal{F}_1 comparing other VLA models, especially in the Handover (R2H) task which requires the dynamic environment understanding capabilities.

3.2 COMPARISON ON THE SIMULATION BENCHMARK

We evaluate \mathcal{F}_1 against various VLA models on two simulation benchmarks: LIBERO (Liu et al., 2023a) and SimplerEnv Bridge (Li et al., 2024b). This comparison specifically aims to demonstrate how \mathcal{F}_1 ’s integrated understanding-generation-action framework, leveraging explicit visual foresight as targets, leads to superior and more robust performance compared to prevailing methods.

LIBERO Benchmark. It evaluates robotic manipulation skills, focusing on spatial and object-centric reasoning, and long-horizon planning. We compare \mathcal{F}_1 with Diffusion Policy (Chi et al., 2023), OpenVLA (Kim et al., 2024), SpatialVLA (Qu et al., 2025b), π_0 (Black et al., 2024), π_0 -Fast (Pertsch et al., 2025), gr00t-N1 (Bjorck et al., 2025), and CoT-VLA (Zhao et al., 2025), using Success Rate (SR) and Ranking (Rank) as primary metrics. As shown in Tab. 2, our proposed model \mathcal{F}_1 consistently achieves superior performance across all suites. This benchmark includes tasks demanding precise spatial understanding, intricate object interaction, goal-oriented execution, and particularly challenging long-horizon sequences. The significant improvement underscores the efficacy of \mathcal{F}_1 ’s unique foresight-guided planning approach, which allows it to transform action generation into a more informed inverse dynamics problem by predicting plausible future visual states. Notably, on the LIBERO-Long tasks, our model exhibits a pronounced advantage over reactive methods. It highlights \mathcal{F}_1 ’s enhanced capability for long-term planning and execution, a direct benefit of its explicit visual foresight.

	Pretrained	LIBERO-Spatial		LIBERO-Object		LIBERO-Goal		LIBERO-Long		Average	
		SR (↑)	Rank (↓)	SR (↑)	Rank (↓)	SR (↑)	Rank (↓)	SR (↑)	Rank (↓)	SR (↑)	Rank (↓)
Diffusion Policy	✗	78.5%	11	87.5%	10	73.5%	11	64.8%	6	76.1%	9
OpenVLA	✓	84.7%	8	88.4%	9	79.2%	9	53.7%	10	76.5%	8
SpatialVLA	✓	88.2%	6	89.9%	8	78.6%	10	55.5%	9	78.1%	7
π_0	✓	98.0%	2	96.8%	4	94.4%	2	88.4%	3	94.4%	2
π_0 -Fast	✓	96.4%	3	96.8%	4	88.6%	5	60.2%	8	85.5%	5
gr00t-N1	✓	94.4%	5	97.6%	1	93.0%	4	90.6%	2	93.9%	4
CoT-VLA	✓	87.5%	7	91.6%	7	87.6%	6	69.0%	4	83.9%	6
\mathcal{F}_1 (Ours)	✗	97.4%	3	97.6%	2	94.2%	3	88.0%	4	94.3%	3
\mathcal{F}_1 (Ours)	✓	98.2%	1	97.8%	1	95.4%	1	91.3%	1	95.7%	1

Table 2: **Results on LIBERO Benchmark.** We report Success Rate (SR, higher is better) and Ranking (Rank, lower is better) across four suites: LIBERO-Spatial, LIBERO-Object, LIBERO-Goal, and LIBERO-Long, as well as the averaged results. The best results are displayed in **bold**.

SimplerEnv Bridge Benchmark. It focuses on complex, multi-step manipulation tasks that often require fine-grained control and precise interaction. We compare \mathcal{F}_1 against RT-1-X (Brohan et al., 2023), RoboVLM (Li et al., 2024a), SpatialVLA, π_0 , and π_0 -Fast, measuring Grasp Success and Overall Success for each task. Tab. 3 shows the performance of our model and other methods. Overall, \mathcal{F}_1 substantially outperforms other models, demonstrating a marked improvement in average success rate compared to the next best baselines. This superior performance is largely attributed to \mathcal{F}_1 ’s enhanced generalization capabilities for precise pick and place positions, which are critical for success in these intricate manipulation scenarios. We induce that unlike reactive policies that might struggle with different source object configurations or target locations, \mathcal{F}_1 ’s foresight mechanism enables it to adapt more effectively.

	Pretrained	Carrot on Plate		Eggplant in Basket		Spoon on Towel		Stack Block		Overall
		Grasp	Success	Grasp	Success	Grasp	Success	Grasp	Success	Average
RT-1-X	✗	20.8%	4.2%	0.0%	0.0%	16.7%	0.0%	8.3%	0.0%	6.3%
RoboVLM	✓	25.0%	25.0%	45.8%	12.5%	58.3%	58.3%	54.2%	29.2%	38.5%
SpatialVLA	✓	29.2%	25.0%	100.0%	100.0%	20.8%	16.7%	62.5%	29.2%	47.9%
π_0	✓	25.0%	0.0%	50.0%	16.6%	91.6%	62.5%	45.8%	29.1%	40.1%
π_0 -Fast	✓	58.5%	21.9%	54.0%	10.8%	83.3%	66.6%	62.5%	29.1%	48.3%
\mathcal{F}_1 (Ours)	✗	70.8%	33.3%	87.5%	75.0%	70.8%	45.8%	83.3%	62.5%	66.1%
\mathcal{F}_1 (Ours)	✓	87.5%	70.8%	100.0%	66.7%	70.8%	50.0%	87.5%	50.0%	72.9%

Table 3: **Results on SimplerEnv Bridge Benchmark.** For each task, we report both *Grasp Success* and *Overall Task Success*, capturing fine-grained control and precise placement capabilities. The last column shows the overall average score, obtained by averaging the success rates of grasping and full task completion across all tasks. The best results are displayed in **bold**.

	LIBERO				SimplerEnv Bridge				Avg
	Spatial	Object	Goal	Long	Carrot	Eggplant	Spoon	Block	
<i>Comparison of \mathcal{F}_1 and its variant which freezes the generation expert during Stage II and III training</i>									
\mathcal{F}_1	98.2%	97.8%	95.4%	91.3%	70.8%	66.7%	50.0%	50.0%	77.5%
(a) Frozen-Gen	95.6%	97.0%	93.6%	87.4%	41.7%	54.2%	45.8%	75.0%	73.8%
<i>Comparison of \mathcal{F}_1 and its variant which is only trained by Stage I and Stage III</i>									
\mathcal{F}_1	98.2%	97.8%	95.4%	91.3%	70.8%	66.7%	50.0%	50.0%	77.5%
(b) Cotrain-Scratch	97.4%	97.6%	94.2%	88.0%	33.3%	75.0%	45.8%	62.5%	74.2%
<i>Comparison of \mathcal{F}_1 and its variant which does not have generation expert</i>									
\mathcal{F}_1	98.2%	97.8%	95.4%	91.3%	70.8%	66.7%	50.0%	50.0%	77.5%
(c) No-Gen	98.0%	96.8%	94.4%	88.4%	0.0 %	16.6%	62.5%	29.1%	60.3%
<i>Comparison of \mathcal{F}_1 and its variant with varying numbers of planning scales</i>									
\mathcal{F}_1 (4-Scales)	98.2%	97.8%	95.4%	91.3%	70.8%	66.7%	50.0%	50.0%	77.5%
(d) 2-Scales	98.0%	97.6%	94.6%	88.6%	29.2%	83.3%	41.7%	54.2%	73.4%
(e) 6-Scales	97.0%	97.2%	94.2%	89.2%	50.0%	87.5%	37.5%	54.2%	75.8%

Table 4: **Ablation Studies on the Simulation Benchmark.** We design five model variants to verify the effects of different components of \mathcal{F}_1 : (a) Frozen-Gen, (b) Cotrain-Scratch, (c) No-Gen, (d) 2-Scales, and (e) 6-Scales.

3.3 ABLATION STUDIES

3.3.1 RESULTS ON THE SIMULATION BENCHMARK

To better understand the individual contributions of foresight prediction and pretraining in \mathcal{F}_1 , we conduct systematic ablations on the LIBERO and SimplerEnv-Bridge benchmarks. We design five model variants to isolate the effects of visual foresight and pretraining under different configurations:

- (a) **Frozen-Gen:** The generation expert is pretrained in Stage I and then frozen during Pretrain Stage II and Post-train Stage III. Its predicted foresight tokens are used as planning cues to guide action prediction, but not used as training targets.
- (b) **Cotrain-Scratch:** The model is trained by Pretrain Stage I and Post-train Stage III, without Pretrain Stage II, i.e., pretraining on large-scale robotic datasets.
- (c) **No-Gen:** The generation expert is entirely removed, resulting in a purely VLA model without any foresight prediction or pretraining.
- (d) **2-Scales:** The fully pretrained model predicts foresight tokens for only two future steps at inference time.
- (e) **6-Scales:** The fully pretrained model predicts foresight tokens for six future steps at inference, evaluating the effect of different scales of intermediate visual representation.

Training vs. Freezing the Generation Expert. To understand the benefits of joint optimization, we compared our model with the (a) Frozen-Gen variant. In this variant, the generation expert was pretrained in Stage I but then kept frozen, preventing it from adapting during subsequent stages. This comparison revealed a moderate performance drop from 77.5% to 73.8% for the Frozen-Gen variant. Moreover, it also confirms that while a fixed, pretrained generation expert can still provide useful planning cues, end-to-end adaptation is crucial for achieving better task alignment. The performance gap indicates that allowing the generation expert to be fine-tuned during later stages enables it to better capture task-specific dynamics. Ultimately, this highlights the significant benefit of jointly optimizing the foresight prediction with the downstream control policy.

Effectiveness of Pretrain. We assess the impact of pretraining by comparing our model with the (b) Cotrain-Scratch variant, which was trained without the large-scale robotics dataset pretraining (Stage II). The removal of this stage results in an overall performance drop of approximately 3.3%. This finding suggests that pretraining on robotics data acts as a crucial inductive prior. It effectively stabilizes the entire optimization process and allows the model to inherit foundational manipulation skills. As a result, our model achieves a higher success rate on downstream tasks by building upon the robust capabilities acquired during the pretraining stage.

Effectiveness of Generation Expert. To evaluate the contribution of the generation expert, we conduct a key ablation study by comparing our full model with the (c) No-Gen variant, where the entire visual foresight branch was removed. As the results in Table 1 show, this operation leads to a significant performance drop from 77.5% to 60.3%. This marked degradation highlights the critical role of the generation expert in providing explicit visual foresight for effective task planning. The absence of foresight signals severely impairs the model’s ability to achieve generalized goal alignment, reducing it to a more reactive policy. These findings conclusively demonstrate that the generation expert provides essential high-level guidance, enabling the policy to move beyond simple reactive behaviors and make more informed, deliberate planning decisions.

Impact of Planning Scales. We assess the impact of the foresight horizon length (planning scales) by comparing our model with variants that used different numbers of future steps for foresight prediction: (d) 2-Scales, (\mathcal{F}_1) 4-Scales, and (e) 6-Scales. As shown in Tab. 4, these models consistently outperform the No-Gen baseline, underscoring the effectiveness of explicit visual foresight as a planning mechanism. While increasing the planning scale from 2 to 6 steps generally improved performance, the 4-Scales configuration struck the optimal balance. This suggests that a planning horizon of four steps provides sufficient temporal abstraction to guide the policy without introducing unnecessary noise or computational overhead, thus yielding the most robust and effective results. This finding highlights the importance of selecting an appropriate planning scale to maximize the benefits of visual foresight.

3.3.2 ABLATION STUDIES ON THE REAL-WORLD TASKS

To further verify the contribution of pretrain and generation which are two key components within \mathcal{F}_1 , we conduct ablation studies on real-world tasks. Specifically, we compare the performance of our complete model \mathcal{F}_1 against two variants:

1. Cotrain-Scratch: the variant of \mathcal{F}_1 which removes the pretraining of Stage II;
2. No-Gen: the variant which removes the foresight-related module, without any pretraining.

The results, as depicted in Fig. 5, provide clear insights into the role of each component. \mathcal{F}_1 consistently outperforms both the Cotrain-Scratch variant and No-Gen across all evaluated tasks. A notable performance gap is observed when comparing \mathcal{F}_1 with No-Gen, underscoring the critical role of the generation expert. For complex tasks such as “Handover (R2H)” and “Mixture”, No-Gen only obtains 40.0% and 60.0% entire success rate, respectively, while our model achieves a much higher success rate of 93.3% and 73.3%. This contrast highlights that the visual foresight provided by the generation expert is essential for handling complex task dynamics and achieving robust goal alignment. Furthermore, the pretraining stage also proves to be a crucial component. When comparing \mathcal{F}_1 with Cotrain-Scratch variant, our model shows a clear performance advantage in many tasks indicating that pretraining on a large robotics dataset provides a strong inductive prior. This prior enables the model to acquire foundational manipulation skills, which significantly improves generalization.

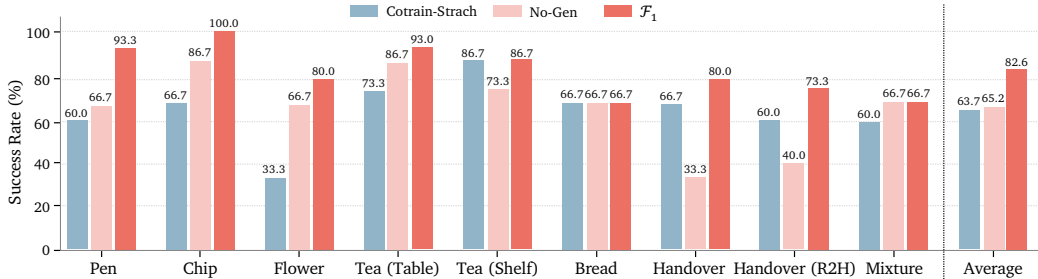


Figure 5: **Ablation Studies on Real-world Tasks.** We compare \mathcal{F}_1 with π_0 as well as a variant that removes Pretrain Stage II. For each task, we conduct 15 trials to ensure statistical reliability. The results show that without Pretrain Stage II, \mathcal{F}_1 suffers a substantial performance drop, even falling below π_0 . In contrast, incorporating Pretrain Stage II leads to marked improvements, with \mathcal{F}_1 significantly surpassing the baseline.

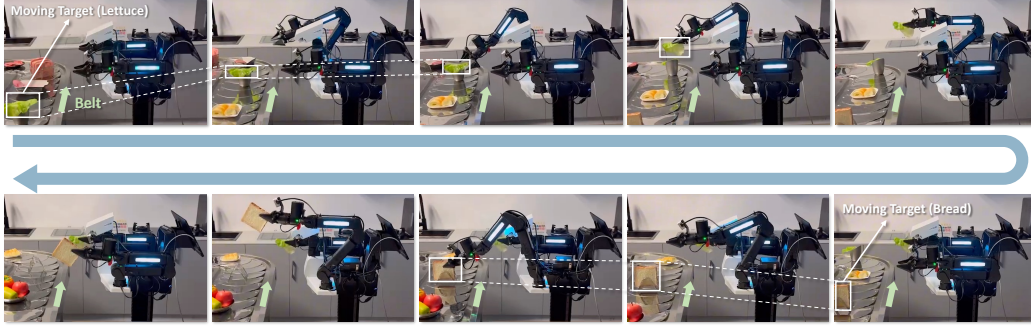


Figure 6: **Visualization of dynamic manipulation task.** A kitchen environment is set up with a moving belt, where the robot must grasp a specified food item according to a language prompt while objects continuously move along the belt.

3.4 ROBUSTNESS AND GENERALIZATION

3.4.1 DYNAMIC ENVIRONMENT

To evaluate \mathcal{F}_1 's robustness, we set up a dynamic manipulation task. As depicted in Fig. 6, we construct a kitchen environment with a moving belt. The robot is required to grasp a specific food item based on a given prompt, while the items are on a moving belt. To further test the model's generalization capabilities, we adopt a novel robot, ARX LIFT II, which is absent from our pretraining dataset. The number of post-train demonstrations is only 47 to explore the shared control capability obtained from pretraining stages.

As shown in Figure 3, our \mathcal{F}_1 achieves a remarkable 66.7% success rate for continuous dual-arm dynamic grasping. For both the "Lettuce" and "Bread" tasks, our model achieves an impressive 80.0% success rate, while π_0 obtains only 53.3% and 46.7%, respectively. This performance stands in stark contrast to the π_0 , which achieves a success rate of only 33.3%. \mathcal{F}_1 's superior performance is directly attributable to its core visual foresight module, which enables it to predict the future position of the moving object and plan its actions accordingly. A detailed breakdown reveals the source of \mathcal{F}_1 's superior performance. It demonstrates that \mathcal{F}_1 effectively leverages its pretrained visual knowledge to generalize to novel embodiments and robustly handle dynamic, real-world challenges.

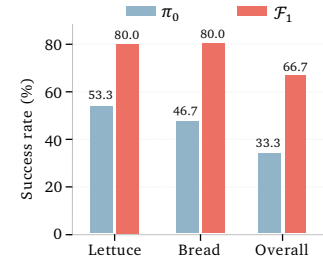


Figure 7: **Results of the Dynamic Manipulation Task.**

3.4.2 ADAPTATION LEARNING

To further validate the generalization capabilities of our model, we conduct two additional sets of experiments, i.e., *sweep* and *sort*, on a Franka robotic arm. For the sweeping task, we evaluate three key performance metrics: the number of objects successfully swept, the maximum number of attempts required to complete the task (capped at five), and the number of empty sweeps. For the sorting task, we measure the success rate over three consecutive grasps.

The results are shown in Tab. 5. In the sweeping task, our model achieves more efficient and reliable interactions, reflected in higher success rates, fewer attempts, and notably fewer empty sweeps. The latter are largely attributable to vertical misalignment, and their reduction indicates more precise spatial grounding during execution. In the sorting task, our model also outperforms π_0 , particularly in the second and third consecutive grasps, where success rates increase substantially. This suggests that \mathcal{F}_1 is better able to sustain performance across repeated interactions, highlighting enhanced robustness in sequential manipulation scenarios.

3.4.3 LONG-HORIZON TASK

To further examine the planning and foresight capabilities of \mathcal{F}_1 , we design a long-horizon manipulation task on the ARX LIFT II platform. This task consists of ten sequential steps and requires

	Sweep			Success Rate of Consecutive Sort		
	# Succ. Objects (\uparrow)	# Max Trials (\downarrow)	# Empty Sweeps (\downarrow)	1st (\uparrow)	2nd (\uparrow)	3rd (\uparrow)
π_0	4.9/8.0	4.8/5.0	2.4/5.0	100.0%	86.7%	53.3%
\mathcal{F}_1	7.1/8.0	3.5/5.0	0.8/5.0	100.0%	100.0%	66.7%

Table 5: **Experimental Results on Franka arm.** The values for the *sweep* task represent the average performance over multiple trials. For the *sort* task, we report the success rate for each of three consecutive grasping attempts.

	① Pickplace Coke \rightarrow	② Pickplace Banana \rightarrow	③ Pour Box \rightarrow	④ Pickup Cloth \rightarrow	⑤ Wipe Table \rightarrow
π_0	93.3%	93.3%	0.0%	0.0%	0.0%
\mathcal{F}_1	100.0%	100.0%	100.0%	93.3%	93.3%

	⑥ Pickup Broom \rightarrow	⑦ Pickup Dustpan \rightarrow	⑧ Sweeping \rightarrow	⑨ Catch Rolling Ball \rightarrow	⑩ Pour Dustpan
π_0	0.0%	0.0%	0.0%	0.0%	0.0%
\mathcal{F}_1	73.3%	60.0%	40.0%	40.0%	40.0%

Table 6: **Step-wise success rates in the long-horizon task.** The task involves ten sequential steps spanning approximately two minutes. Each column reports the average success rate of a specific step across 15 trials. π_0 struggles beyond the first 4 stages, while \mathcal{F}_1 achieves consistently high success rates in early steps and maintains non-trivial performance across later more complex stages.

approximately two minutes to complete. Unlike short episodic interactions, the long-horizon setting places greater demands on temporal consistency, error recovery, and the ability to sustain goal-directed behavior across multiple stages. By evaluating under this setup, we aim to assess whether the foresight-guided mechanism in \mathcal{F}_1 can support coherent action sequences over extended durations, thereby testing its robustness in realistic, temporally extended scenarios.

The results in Tab. 6 reveal a stark contrast between the baseline and our model. The baseline policy π_0 can complete only the simplest grasping actions, but consistently fails when confronted with more complex interactions such as pouring, wiping, or multi-object coordination. In contrast, \mathcal{F}_1 achieves near-perfect performance in the initial stages and sustains meaningful success rates throughout the later steps. Although its performance gradually decreases as the sequence progresses, this trend is expected in long-horizon scenarios due to error accumulation and the compounding difficulty of temporally extended reasoning. The ability of \mathcal{F}_1 to complete the majority of the ten steps, while maintaining robustness over a two-minute execution horizon, highlights its capacity for foresight-guided planning and resilience in sequential, real-world tasks.

4 RELATIONSHIPS BETWEEN GENERATION QUALITY AND ACTIONS

In \mathcal{F}_1 , the generation expert acts as a visual planner, and the quality of its foresight images is crucial for ensuring the reliability of the action expert. To investigate this relationship, we perform a two-step analysis. First, we assess the foresight image quality using a set of predefined evaluation metrics. Second, we study the correlation between generation quality and action prediction by examining token-level accuracy.

4.1 QUANTITATIVE ANALYSIS OF GENERATION

Unlike conventional image-generation works that emphasize pixel-level or distribution-level metrics, e.g. FID (Heusel et al., 2018), or PSNR, our objective is not merely to measure visual realism, but to evaluate whether generated future observations provide actionable guidance for downstream control. To this end, we design a multimodal evaluation protocol based on a large vision-language model, Qwen2.5-VL-32B-Instruct (Bai et al., 2025).

The evaluator receives a task instruction, four historical frames of the robot executing the task, one predicted next-step frame, and the ground-truth frame. The detailed prompt template is included in Appendix E. The evaluation targets three dimensions directly related to action feasibility:

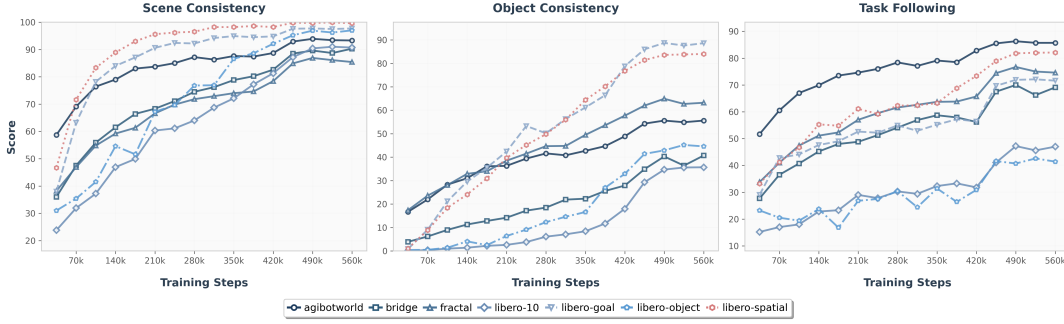


Figure 8: **Generation Quality across Training Steps.** We report the evolution of generation quality along three dimensions: scene consistency (left), object consistency (middle), and task progress following (right). The x-axis denotes training steps, and different curves correspond to distinct task subsets (AgibotWorld, Bridge, Fractal, and LIBERO). Higher scores indicate a better alignment between the generated future observations and the ground-truth task progression.

1. **Scene Consistency:** Whether the global environment remains coherent in layout, lighting, and texture, with blurry or structurally incoherent generations penalized.
2. **Object Consistency:** Whether manipulated objects and the robot remain consistent in identity and spatial position, penalizing missing, deformed, or hallucinated objects.
3. **Task Progress Following:** Whether the generated frame depicts a plausible next step toward fulfilling the instruction, consistent with the ground-truth trajectory.

Each aspect is scored in a binary manner (0/1), and the aggregated score forms our measure of generation quality. This design explicitly ties evaluation to task relevance, enabling us to study how higher-quality generations correlate with improved action execution. Fig. 8 shows that the model’s visual planning capabilities develop hierarchically. **Scene Consistency** improves rapidly at early stages, indicating that global coherence is easier to acquire. **Object Consistency**, however, presents a major challenge: without pretraining on large-scale object-centric datasets, the model struggles to preserve fine-grained shapes and positions, resulting in flatter curves and lower scores throughout training. Despite this weakness, **Task Progress Following** improves steadily and often surpasses object consistency, suggesting that the model captures high-level temporal task logic even without pixel-perfect object representation. This finding highlights the ability of generation expert to generate actionable foresight images, which is ultimately more critical for downstream control than exact visual fidelity.

4.2 QUALITATIVE ANALYSIS OF GENERATION

In addition to the quantitative evaluation, we further conduct a qualitative analysis to gain deeper insights into the strengths and limitations of the generation expert. Fig. 9 presents representative examples of generated foresight images across diverse tasks, such as supermarket manipulation, and clothing folding. Overall, the predicted frames capture task-level plausibility and remain aligned with the ground-truth trajectories, suggesting that the model internalizes a temporal understanding of task logic rather than merely memorizing visual appearances. This ability to generate plausible next-step states highlights the role of the generation expert as a visual planner.

At the same time, we observe clear limitations in visual fidelity, particularly in cases involving fine-grained object details or deformable objects, e.g., grid-shape shopping cart, plastic bags, and clothing. A key reason for this weakness is that our model has not been pretrained on large-scale generative datasets, making it more difficult to preserve precise object shapes and textures. Nevertheless, these imperfections rarely prevent the predictions from providing actionable guidance for downstream control, since the generated frames still convey the essential task progression. These qualitative observations complement our quantitative results: while pixel-level precision remains challenging, the generation expert consistently produces foresight images which are sufficiently informative to support action planning.

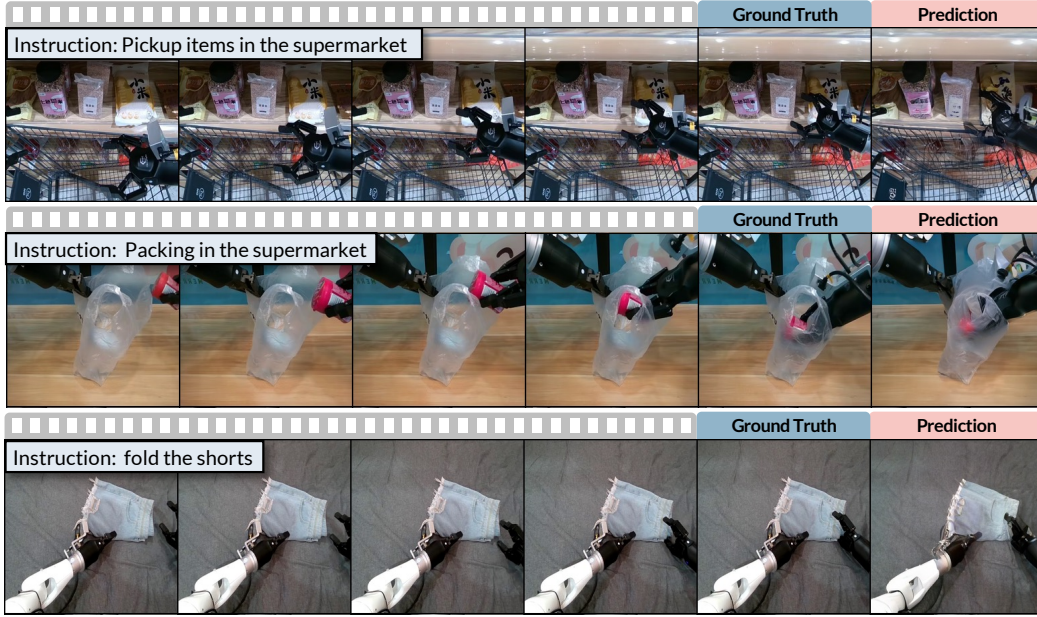


Figure 9: **Visualization of Generated Future Images.** It demonstrates the ability of \mathcal{F}_1 to generate plausible next-step frames for various manipulation tasks, including supermarket item pickup, supermarket packing, and folding shorts. Each row compares a Ground Truth frame with a Prediction from \mathcal{F}_1 , showcasing its accurate foresight across diverse scenarios.

4.3 CORRELATION BETWEEN GENERATION AND ACTIONS

To further study the connection between generation quality and action reliability, we perform controlled experiments on the LIBERO benchmark (Liu et al., 2023a). During training, our model jointly optimizes two objectives: (i) the next visual state through next-scale prediction, and (ii) the action via flow matching. To measure progress on these two objectives, we employ accuracy metrics for both the image and action modalities.

For the image modality, we adopt a Residual VQ-VAE representation, which formulates image prediction as a token-level classification problem. Accordingly, we measure image token accuracy, defined as the classification accuracy of predicted visual tokens against the ground truth tokens; For the action modality, we compute the action token accuracy via:

$$\text{Acc}_\tau = \frac{1}{N} \sum_{t=1}^N [\|\hat{a}_t - a_t\| < \tau], \quad (5)$$

where N is the total number of action tokens and τ denotes the error tolerance threshold. Since training is performed at the chunk level, we evaluate accuracy under the same granularity.

Fig. 10 illustrates the relationship between image token accuracy and action token accuracy across four LIBERO suites. Across all error tolerance levels ($\tau=0.01, 0.02, 0.05$), we observe a consistent positive correlation, confirming that improvements in visual foresight are closely aligned with improvements in action prediction. Notably, the absolute value of image token accuracy remains relatively low (around 40–45% on average). This limitation arises from the fact that our model is not pretrained on large-scale generative datasets, which makes fine-grained token prediction particularly challenging. Nevertheless, even with imperfect image token accuracy, the generated foresight provides sufficient task-relevant cues for the action expert, leading to high action token accuracy.

These results highlight two important insights:

1. Pixel-level image prediction is not strictly necessary for effective action planning: even when the average image token accuracy remains modest, the generated foresight still conveys sufficient task-level cues to support high action accuracy.

2. The strong positive correlation indicates that improvements in image token prediction are reflected in action reliability. Thus, while pixel fidelity is not required, advancing the quality of visual token prediction remains a promising way to enhance downstream action performance.

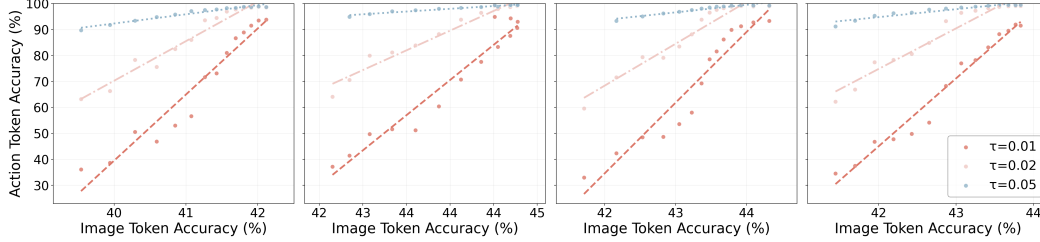


Figure 10: **Correlation between Image and Action Token Accuracy.** It shows the relationship between image token accuracy and action token accuracy across the four LIBERO suites. Each sub-figure corresponds to one suite, and action accuracy is reported at different tolerance levels ($\tau=0.01, 0.02, 0.05$). The consistent positive correlation across all settings suggests that higher-quality visual foresight is closely aligned with improved action prediction reliability.

5 RELATED WORK

5.1 VISION LANGUAGE ACTION MODEL

The rapid progress of multimodal large language models (MLLMs) (Liu et al., 2023b; OpenAI et al., 2024; Yang et al., 2025a; Bai et al., 2025) has motivated the development of Vision Language Action (VLA) models. VLA models incorporate a vision language model and augment it with an action prediction module (Black et al., 2024; Kim et al., 2024; Qu et al., 2025b; Song et al., 2025; Team et al., 2025a; Cheang et al., 2025; Bjorck et al., 2025; Yang et al., 2025b; Bu et al., 2025; Qu et al., 2025a). They leverage the strong perceptual and linguistic grounding of pretrained VLMs, allowing robots to interpret human instructions more flexibly than purely reactive policies. Despite this promise, current VLA models remain limited in robustness. Most formulations still predict actions reactively from the current state without reasoning about how the scene may evolve, leading to short-sighted behavior in dynamic and long-horizon tasks. Despite some studies having attempted to incorporate temporal memory (Li et al., 2025a; Shi et al., 2025) and post-train VLA with reinforcement learning methods (Zhang et al., 2025b; Lu et al., 2025), they still struggle to cope with complex scenarios. In contrast, we propose a unified VLA model which integrates the visual foresight generation into the decision-making pipeline, thereby enhancing its robustness capability.

5.2 INVERSE DYNAMICS MODEL

Since directly mapping the visual observation and textual instruction to action space is a challenge, prior studies (Deng et al., 2025b; Hu et al., 2024; Liao et al., 2025b; Zhong et al., 2025; Cen et al., 2025; Wang et al., 2025; Zhao et al., 2025; Gao et al., 2025) explore to enhance action prediction by injecting auxiliary intermediate representations during training, e.g., grasping poses, segmentation masks, optical flow, or future images, to guide the model toward more structured outputs. However, these representations are often domain-specific and do not fully leverage the potential competence of the pretrained large language model, leaving the policies brittle when deployed beyond their training distributions. **Inverse dynamics model** (Du et al., 2023) can extract the underlying actions from two consecutive images, thereby decreasing the difficulty of mapping from image space to action space. Recent works (Black et al., 2023; Li et al., 2025b; Zhu et al., 2025; Cen et al., 2025; Zhao et al., 2025; Wang et al., 2025; Zhang et al., 2025a) attempt to decompose the decision-making task to first generate future images or videos, and then predict actions. Nevertheless, they mostly use the future prediction objective as a regularizer when training, but seldom generate the visual guidance during the inference stage. In contrast, our model first predicts the next frame and then predicts the action conditioned on the predicted visual foresight, improving the robustness and generalization.

5.3 UNIFIED VISION LANGUAGE MODEL

Building on MLLMs, recent research explores unified models that combine visual understanding and generation within a single framework. Early approaches (Lu et al., 2023; Zhou et al., 2024; Xie et al., 2024; Wang et al., 2024) employ discrete visual tokenization to enable joint modeling, but suffer from information loss and weakened semantics. While a line of works (Wu et al., 2024; Pan et al., 2025; Chen et al., 2025; Lin et al., 2025) adopt modular assemblies of pretrained MLLMs and diffusion models, sacrificing true unification. More recent efforts (Deng et al., 2025a; Liao et al., 2025a) introduce Mixture-of-Transformers (MoT) architectures with separate experts for text and visual generation, but still inherit the latency of diffusion and reliance on external encoders. However, existing unified frameworks remain centered on visual understanding and generation, leaving action outside the scope of cognitive intelligence. From the perspective of embodied AI, we argue that **intelligence requires not only perceiving and imagining but also interacting with the physical world**. Compared to understanding or generation, action is inherently more complex and demanding. This motivates us to extend the unified paradigm toward an understanding generation action framework, enabling agents to achieve a more complete form of cognitive intelligence.

6 CONCLUSION AND FUTURE WORK

This paper has introduced \mathcal{F}_1 , a pretrained Vision-Language-Action (VLA) framework that integrates goal-conditioned visual foresight into the perception-action loop. Building on the principle of predictive inverse dynamics, \mathcal{F}_1 reformulates control as foresight-guided inverse dynamics, allowing actions to be derived not only from the current state but also from an anticipated visual outcome. Architecturally, the model adopts a Mixture-of-Transformer design with three dedicated experts for understanding, foresight generation, and action execution, while a next-scale prediction mechanism and progressive attention scheme regulate the flow of information across modules. To further enhance robustness and transferability, we introduced a three-stage training recipe that progressively aligns, pretrains, and adapts the experts on large-scale and task-specific robot datasets. Extensive experiments across simulation benchmarks and physical platforms demonstrate that \mathcal{F}_1 consistently surpasses reactive baselines, achieving higher success rates and improved generalization in dynamic and long-horizon tasks.

Beyond the reported performance gains, this work integrates predictive foresight with multimodal grounding in a unified VLA framework. The modular architecture adapts large-scale vision-language backbones to robotic control and incorporates dedicated experts for understanding, foresight generation, and action execution. In parallel, the progressive training scheme offers a systematic way to align and integrate these components, ensuring that foresight signals remain consistent with semantic grounding while supporting transfer across tasks and embodiments. This combination contributes to policies that are less dependent on purely reactive mappings and better suited to dynamic and long-horizon scenarios. More broadly, the study provides evidence that coupling foresight with multimodal grounding is a viable direction for advancing robust visuomotor control.

Several avenues remain for future investigation. Scaling foresight-driven policies to more diverse embodiments and task families, e.g., locomotion, dexterous manipulation, or multi-agent collaboration, would provide a stronger test of generality. Another direction is to enrich the foresight generation module with structured world models or physics-informed priors, enabling more accurate long-horizon reasoning and robustness under distributional shift. Integrating reinforcement learning or online adaptation strategies with foresight-guided architectures may further allow agents to refine policies beyond imitation, supporting continual improvement in open-ended environments. Finally, exploring how human feedback or interactive correction can be incorporated into foresight-driven policies presents an opportunity to align embodied agents more closely with human intentions.

REFERENCES

AgiBot-World-Contributors, Qingwen Bu, Jisong Cai, Li Chen, Xiuqi Cui, Yan Ding, Siyuan Feng, Shenyuan Gao, Xindong He, Xuan Hu, Xu Huang, Shu Jiang, Yuxin Jiang, Cheng Jing, Hongyang Li, Jialu Li, Chiming Liu, Yi Liu, Yuxiang Lu, Jianlan Luo, Ping Luo, Yao Mu, Yuehan Niu, Yixuan Pan, Jiangmiao Pang, Yu Qiao, Guanghui Ren, Cheng Ruan, Jiaqi Shan, Yongjian Shen, Chengshi Shi, Mingkan Shi, Modi Shi, Chonghao Sima, Jianheng Song, Huijie Wang, Wenhao

- Wang, Dafeng Wei, Chengen Xie, Guo Xu, Junchi Yan, Cunbiao Yang, Lei Yang, Shukai Yang, Maoqing Yao, Jia Zeng, Chi Zhang, Qinglin Zhang, Bin Zhao, Chengyue Zhao, Jiaqi Zhao, and Jianchao Zhu. Agibot world colosseo: A large-scale manipulation platform for scalable and intelligent embodied systems, 2025. URL <https://arxiv.org/abs/2503.06669>.
- Shuai Bai, Keqin Chen, Xuejing Liu, Jialin Wang, Wenbin Ge, Sibao Song, Kai Dang, Peng Wang, Shijie Wang, Jun Tang, Humen Zhong, Yuanzhi Zhu, Mingkun Yang, Zhaohai Li, Jianqiang Wan, Pengfei Wang, Wei Ding, Zheren Fu, Yiheng Xu, Jiabo Ye, Xi Zhang, Tianbao Xie, Zesen Cheng, Hang Zhang, Zhibo Yang, Haiyang Xu, and Junyang Lin. Qwen2.5-vl technical report, 2025. URL <https://arxiv.org/abs/2502.13923>.
- Lucas Beyer, Andreas Steiner, André Susano Pinto, Alexander Kolesnikov, Xiao Wang, Daniel Salz, Maxim Neumann, Ibrahim Alabdulmohsin, Michael Tschannen, Emanuele Bugliarello, Thomas Unterthiner, Daniel Keysers, Skanda Koppula, Fangyu Liu, Adam Grycner, Alexey Gritsenko, Neil Houlsby, Manoj Kumar, Keran Rong, Julian Eisenschlos, Rishabh Kabra, Matthias Bauer, Matko Bošnjak, Xi Chen, Matthias Minderer, Paul Voigtlaender, Ioana Bica, Ivana Balazevic, Joan Puigcerver, Pinelopi Papalampidi, Olivier Henaff, Xi Xiong, Radu Soricut, Jeremiah Harmsen, and Xiaohua Zhai. Paligemma: A versatile 3b vlm for transfer, 2024. URL <https://arxiv.org/abs/2407.07726>.
- Johan Bjorck, Fernando Castañeda, Nikita Cherniadev, Xingye Da, Runyu Ding, Linxi Fan, Yu Fang, Dieter Fox, Fengyuan Hu, Spencer Huang, et al. Gr00t n1: An open foundation model for generalist humanoid robots. *arXiv preprint arXiv:2503.14734*, 2025.
- Kevin Black, Mitsuhiko Nakamoto, Pranav Atreya, Homer Walke, Chelsea Finn, Aviral Kumar, and Sergey Levine. Zero-shot robotic manipulation with pretrained image-editing diffusion models, 2023. URL <https://arxiv.org/abs/2310.10639>.
- Kevin Black, Noah Brown, Danny Driess, Adnan Esmail, Michael Equi, Chelsea Finn, Niccolo Fusai, Lachy Groom, Karol Hausman, Brian Ichter, et al. π_0 : A vision-language-action flow model for general robot control. *arXiv preprint arXiv:2410.24164*, 2024.
- Anthony Brohan, Noah Brown, Justice Carbajal, Yevgen Chebotar, Joseph Dabis, Chelsea Finn, Keerthana Gopalakrishnan, Karol Hausman, Alex Herzog, Jasmine Hsu, Julian Ibarz, Brian Ichter, Alex Irpan, Tomas Jackson, Sally Jesmonth, Nikhil J Joshi, Ryan Julian, Dmitry Kalashnikov, Yuheng Kuang, Isabel Leal, Kuang-Huei Lee, Sergey Levine, Yao Lu, Utsav Malla, Deeksha Manjunath, Igor Mordatch, Ofir Nachum, Carolina Parada, Jodilyn Peralta, Emily Perez, Karl Pertsch, Jornell Quiambao, Kanishka Rao, Michael Ryoo, Grecia Salazar, Pannag Sanketi, Kevin Sayed, Jaspiar Singh, Sumedh Sontakke, Austin Stone, Clayton Tan, Huong Tran, Vincent Vanhoucke, Steve Vega, Quan Vuong, Fei Xia, Ted Xiao, Peng Xu, Sichun Xu, Tianhe Yu, and Brianna Zitkovich. Rt-1: Robotics transformer for real-world control at scale, 2023. URL <https://arxiv.org/abs/2212.06817>.
- Qingwen Bu, Yanting Yang, Jisong Cai, Shenyuan Gao, Guanghui Ren, Maoqing Yao, Ping Luo, and Hongyang Li. Univla: Learning to act anywhere with task-centric latent actions, 2025. URL <https://arxiv.org/abs/2505.06111>.
- Jun Cen, Chaohui Yu, Hangjie Yuan, Yuming Jiang, Siteng Huang, Jiayan Guo, Xin Li, Yibing Song, Hao Luo, Fan Wang, Deli Zhao, and Hao Chen. Worldvla: Towards autoregressive action world model, 2025. URL <https://arxiv.org/abs/2506.21539>.
- Chilam Cheang, Sijin Chen, Zhongren Cui, Yingdong Hu, Liqun Huang, Tao Kong, Hang Li, Yifeng Li, Yuxiao Liu, Xiao Ma, Hao Niu, Wenxuan Ou, Wanli Peng, Zeyu Ren, Haixin Shi, Jiawen Tian, Hongtao Wu, Xin Xiao, Yuyang Xiao, Jiafeng Xu, and Yichu Yang. Gr-3 technical report, 2025. URL <https://arxiv.org/abs/2507.15493>.
- Jiuhai Chen, Zhiyang Xu, Xichen Pan, Yushi Hu, Can Qin, Tom Goldstein, Lifu Huang, Tianyi Zhou, Saining Xie, Silvio Savarese, Le Xue, Caiming Xiong, and Ran Xu. Blip3-o: A family of fully open unified multimodal models-architecture, training and dataset, 2025. URL <https://arxiv.org/abs/2505.09568>.

Cheng Chi, Zhenjia Xu, Siyuan Feng, Eric Cousineau, Yilun Du, Benjamin Burchfiel, Russ Tedrake, and Shuran Song. Diffusion policy: Visuomotor policy learning via action diffusion. *arXiv preprint arXiv:2303.04137*, 2023.

Embodiment Collaboration, Abby O’Neill, Abdul Rehman, Abhinav Gupta, Abhiram Maddukuri, Abhishek Gupta, Abhishek Padalkar, Abraham Lee, Acorn Pooley, Agrim Gupta, Ajay Mandelkar, Ajinkya Jain, Albert Tung, Alex Bewley, Alex Herzog, Alex Irpan, Alexander Khazatsky, Anant Rai, Anchit Gupta, Andrew Wang, Andrey Kolobov, Anikait Singh, Animesh Garg, Aniruddha Kembhavi, Annie Xie, Anthony Brohan, Antonin Raffin, Archit Sharma, Arefeh Yavary, Arhan Jain, Ashwin Balakrishna, Ayzaan Wahid, Ben Burgess-Limerick, Beomjoon Kim, Bernhard Schölkopf, Blake Wulfe, Brian Ichter, Cewu Lu, Charles Xu, Charlotte Le, Chelsea Finn, Chen Wang, Chenfeng Xu, Cheng Chi, Chenguang Huang, Christine Chan, Christopher Agia, Chuer Pan, Chuyuan Fu, Coline Devin, Danfei Xu, Daniel Morton, Danny Driess, Daphne Chen, Deepak Pathak, Dhruv Shah, Dieter Buechler, Dinesh Jayaraman, Dmitry Kalashnikov, Dorsa Sadigh, Edward Johns, Ethan Foster, Fangchen Liu, Federico Ceola, Fei Xia, Feiyu Zhao, Felipe Vieira Frujeri, Freek Stulp, Gaoyue Zhou, Gaurav S. Sukhatme, Gautam Salhotra, Ge Yan, Gilbert Feng, Giulio Schiavi, Glen Berseth, Gregory Kahn, Guangwen Yang, Guanzhi Wang, Hao Su, Hao-Shu Fang, Haochen Shi, Henghui Bao, Heni Ben Amor, Henrik I Christensen, Hiroki Furuta, Homanga Bharadhwaj, Homer Walke, Hongjie Fang, Huy Ha, Igor Mordatch, Ilija Radosavovic, Isabel Leal, Jacky Liang, Jad Abou-Chakra, Jaehyung Kim, Jaimyn Drake, Jan Peters, Jan Schneider, Jasmine Hsu, Jay Vakil, Jeannette Bohg, Jeffrey Bingham, Jeffrey Wu, Jensen Gao, Jiaheng Hu, Jiajun Wu, Jialin Wu, Jiankai Sun, Jianlan Luo, Jiayuan Gu, Jie Tan, Jihoon Oh, Jimmy Wu, Jingpei Lu, Jingyun Yang, Jitendra Malik, João Silvério, Joey Hejna, Jonathan Booyer, Jonathan Tompson, Jonathan Yang, Jordi Salvador, Joseph J. Lim, Junhyek Han, Kaiyuan Wang, Kanishka Rao, Karl Pertsch, Karol Hausman, Kegan Go, Keerthana Gopalakrishnan, Ken Goldberg, Kendra Byrne, Kenneth Oslund, Kento Kawaharazuka, Kevin Black, Kevin Lin, Kevin Zhang, Kiana Ehsani, Kiran Lekkala, Kirsty Ellis, Krishan Rana, Krishnan Srinivasan, Kuan Fang, Kunal Pratap Singh, Kuo-Hao Zeng, Kyle Hatch, Kyle Hsu, Laurent Itti, Lawrence Yunliang Chen, Lerrel Pinto, Li Fei-Fei, Liam Tan, Linxi ”Jim” Fan, Lionel Ott, Lisa Lee, Luca Weihs, Magnum Chen, Marion Lepert, Marius Memmel, Masayoshi Tomizuka, Masha Itkina, Mateo Guaman Castro, Max Spero, Maximilian Du, Michael Ahn, Michael C. Yip, Mingtong Zhang, Mingyu Ding, Minh Ho, Mohan Kumar Srirama, Mohit Sharma, Moo Jin Kim, Muhammad Zubair Irshad, Naoaki Kanazawa, Nicklas Hansen, Nicolas Heess, Nikhil J Joshi, Niko Suenderhauf, Ning Liu, Norman Di Palo, Nur Muhammad Mahi Shafiullah, Oier Mees, Oliver Kroemer, Osbert Bastani, Pannag R Sanketi, Patrick ”Tree” Miller, Patrick Yin, Paul Wohlhart, Peng Xu, Peter David Fagan, Peter Mitrano, Pierre Sermanet, Pieter Abbeel, Priya Sundaresan, Qiuyu Chen, Quan Vuong, Rafael Rafailov, Ran Tian, Ria Doshi, Roberto Martín-Martín, Rohan Bajjal, Rosario Scalise, Rose Hendrix, Roy Lin, Runjia Qian, Ruohan Zhang, Russell Mendonca, Rutav Shah, Ryan Hoque, Ryan Julian, Samuel Bustamante, Sean Kirmani, Sergey Levine, Shan Lin, Sherry Moore, Shikhar Bahl, Shivin Dass, Shubham Sonawani, Shubham Tulsiani, Shuran Song, Sichun Xu, Siddhant Halder, Siddharth Karamcheti, Simeon Adebola, Simon Guist, Soroush Nasiriany, Stefan Schaal, Stefan Welker, Stephen Tian, Subramanian Ramamoorthy, Sudeep Dasari, Suneel Belkale, Sungjae Park, Suraj Nair, Suvir Mirchandani, Takayuki Osa, Tanmay Gupta, Tatsuya Harada, Tatsuya Matsushima, Ted Xiao, Thomas Kollar, Tianhe Yu, Tianli Ding, Todor Davchev, Tony Z. Zhao, Travis Armstrong, Trevor Darrell, Trinity Chung, Vidhi Jain, Vikash Kumar, Vincent Vanhoucke, Vitor Guizilini, Wei Zhan, Wenxuan Zhou, Wolfram Burgard, Xi Chen, Xiangyu Chen, Xiaolong Wang, Xinghao Zhu, Xinyang Geng, Xiyuan Liu, Xu Liangwei, Xuanlin Li, Yansong Pang, Yao Lu, Yecheng Jason Ma, Yejin Kim, Yevgen Chebotar, Yifan Zhou, Yifeng Zhang, Yilun Wu, Ying Xu, Yixuan Wang, Yonatan Bisk, Yongqiang Dou, Yoonyoung Cho, Youngwoon Lee, Yuchen Cui, Yue Cao, Yueh-Hua Wu, Yujin Tang, Yuke Zhu, Yunchu Zhang, Yunfan Jiang, Yunshuang Li, Yunzhu Li, Yusuke Iwasawa, Yutaka Matsuo, Zehan Ma, Zhuo Xu, Zichen Jeff Cui, Zichen Zhang, Zipeng Fu, and Zipeng Lin. Open x-embodiment: Robotic learning datasets and rt-x models, 2025. URL <https://arxiv.org/abs/2310.08864>.

Chaorui Deng, Deyao Zhu, Kunchang Li, Chenhui Gou, Feng Li, Zeyu Wang, Shu Zhong, Weihao Yu, Xiaonan Nie, Ziang Song, Guang Shi, and Haoqi Fan. Emerging properties in unified multimodal pretraining, 2025a. URL <https://arxiv.org/abs/2505.14683>.

- Shengliang Deng, Mi Yan, Songlin Wei, Haixin Ma, Yuxin Yang, Jiayi Chen, Zhiqi Zhang, Taoyu Yang, Xuheng Zhang, Wenhao Zhang, Heming Cui, Zhizheng Zhang, and He Wang. Graspvla: a grasping foundation model pre-trained on billion-scale synthetic action data, 2025b. URL <https://arxiv.org/abs/2505.03233>.
- Yilun Du, Mengjiao Yang, Bo Dai, Hanjun Dai, Ofir Nachum, Joshua B. Tenenbaum, Dale Schuurmans, and Pieter Abbeel. Learning universal policies via text-guided video generation, 2023. URL <https://arxiv.org/abs/2302.00111>.
- Chongkai Gao, Haozhuo Zhang, Zhixuan Xu, Zhehao Cai, and Lin Shao. Flip: Flow-centric generative planning as general-purpose manipulation world model, 2025. URL <https://arxiv.org/abs/2412.08261>.
- Martin Heusel, Hubert Ramsauer, Thomas Unterthiner, Bernhard Nessler, and Sepp Hochreiter. Gans trained by a two time-scale update rule converge to a local nash equilibrium, 2018. URL <https://arxiv.org/abs/1706.08500>.
- Yucheng Hu, Yanjiang Guo, Pengchao Wang, Xiaoyu Chen, Yen-Jen Wang, Jianke Zhang, Koushil Sreenath, Chaochao Lu, and Jianyu Chen. Video prediction policy: A generalist robot policy with predictive visual representations. *arXiv preprint arXiv:2412.14803*, 2024.
- Moo Jin Kim, Karl Pertsch, Siddharth Karamcheti, Ted Xiao, Ashwin Balakrishna, Suraj Nair, Rafael Rafailov, Ethan Foster, Grace Lam, Pannag Sanketi, Quan Vuong, Thomas Kollar, Benjamin Burchfiel, Russ Tedrake, Dorsa Sadigh, Sergey Levine, Percy Liang, and Chelsea Finn. Openvla: An open-source vision-language-action model, 2024. URL <https://arxiv.org/abs/2406.09246>.
- Doyup Lee, Chiheon Kim, Saehoon Kim, Minsu Cho, and Wook-Shin Han. Autoregressive image generation using residual quantization, 2022. URL <https://arxiv.org/abs/2203.01941>.
- Hao Li, Shuai Yang, Yilun Chen, Yang Tian, Xiaoda Yang, Xinyi Chen, Hanqing Wang, Tai Wang, Feng Zhao, Dahua Lin, and Jiangmiao Pang. Cronusvla: Transferring latent motion across time for multi-frame prediction in manipulation, 2025a. URL <https://arxiv.org/abs/2506.19816>.
- Shuang Li, Yihuai Gao, Dorsa Sadigh, and Shuran Song. Unified video action model, 2025b. URL <https://arxiv.org/abs/2503.00200>.
- Xinghang Li, Peiyan Li, Minghuan Liu, Dong Wang, Jirong Liu, Bingyi Kang, Xiao Ma, Tao Kong, Hanbo Zhang, and Huaping Liu. Towards generalist robot policies: What matters in building vision-language-action models, 2024a. URL <https://arxiv.org/abs/2412.14058>.
- Xuanlin Li, Kyle Hsu, Jiayuan Gu, Karl Pertsch, Oier Mees, Homer Rich Walke, Chuyuan Fu, Ishikaa Lunawat, Isabel Sieh, Sean Kirmani, Sergey Levine, Jiajun Wu, Chelsea Finn, Hao Su, Quan Vuong, and Ted Xiao. Evaluating real-world robot manipulation policies in simulation, 2024b. URL <https://arxiv.org/abs/2405.05941>.
- Weixin Liang, Lili Yu, Liang Luo, Srinivasan Iyer, Ning Dong, Chunting Zhou, Gargi Ghosh, Mike Lewis, Wen tau Yih, Luke Zettlemoyer, and Xi Victoria Lin. Mixture-of-transformers: A sparse and scalable architecture for multi-modal foundation models, 2025. URL <https://arxiv.org/abs/2411.04996>.
- Chao Liao, Liyang Liu, Xun Wang, Zhengxiong Luo, Xinyu Zhang, Wenliang Zhao, Jie Wu, Liang Li, Zhi Tian, and Weilin Huang. Mogao: An omni foundation model for interleaved multi-modal generation, 2025a. URL <https://arxiv.org/abs/2505.05472>.
- Yue Liao, Pengfei Zhou, Siyuan Huang, Donglin Yang, Shengcong Chen, Yuxin Jiang, Yue Hu, Jingbin Cai, Si Liu, Jianlan Luo, et al. Genie envisioner: A unified world foundation platform for robotic manipulation. *arXiv preprint arXiv:2508.05635*, 2025b.

- Bin Lin, Zongjian Li, Xinhua Cheng, Yuwei Niu, Yang Ye, Xianyi He, Shenghai Yuan, Wangbo Yu, Shaodong Wang, Yunyang Ge, Yatian Pang, and Li Yuan. Uniworld-v1: High-resolution semantic encoders for unified visual understanding and generation, 2025. URL <https://arxiv.org/abs/2506.03147>.
- Yaron Lipman, Ricky T. Q. Chen, Heli Ben-Hamu, Maximilian Nickel, and Matt Le. Flow matching for generative modeling, 2023. URL <https://arxiv.org/abs/2210.02747>.
- Bo Liu, Yifeng Zhu, Chongkai Gao, Yihao Feng, Qiang Liu, Yuke Zhu, and Peter Stone. Libero: Benchmarking knowledge transfer for lifelong robot learning, 2023a. URL <https://arxiv.org/abs/2306.03310>.
- Haotian Liu, Chunyuan Li, Qingyang Wu, and Yong Jae Lee. Visual instruction tuning, 2023b. URL <https://arxiv.org/abs/2304.08485>.
- Guanxing Lu, Wenkai Guo, Chubin Zhang, Yuheng Zhou, Haonan Jiang, Zifeng Gao, Yansong Tang, and Ziwei Wang. Vla-rl: Towards masterful and general robotic manipulation with scalable reinforcement learning, 2025. URL <https://arxiv.org/abs/2505.18719>.
- Pan Lu, Baolin Peng, Hao Cheng, Michel Galley, Kai-Wei Chang, Ying Nian Wu, Song-Chun Zhu, and Jianfeng Gao. Chameleon: Plug-and-play compositional reasoning with large language models, 2023. URL <https://arxiv.org/abs/2304.09842>.
- OpenAI, Josh Achiam, Steven Adler, Sandhini Agarwal, Lama Ahmad, Ilge Akkaya, Florencia Leoni Aleman, Diogo Almeida, Janko Altschmidt, Sam Altman, Shyamal Anadkat, Red Avila, Igor Babuschkin, Suchir Balaji, Valerie Balcom, Paul Baltescu, Haiming Bao, Mohammad Bavarian, Jeff Belgum, Irwan Bello, Jake Berdine, Gabriel Bernadett-Shapiro, Christopher Berner, Lenny Bogdonoff, Oleg Boiko, Madelaine Boyd, Anna-Luisa Brakman, Greg Brockman, Tim Brooks, Miles Brundage, Kevin Button, Trevor Cai, Rosie Campbell, Andrew Cann, Brittany Carey, Chelsea Carlson, Rory Carmichael, Brooke Chan, Che Chang, Fotis Chantzis, Derek Chen, Sully Chen, Ruby Chen, Jason Chen, Mark Chen, Ben Chess, Chester Cho, Casey Chu, Hyung Won Chung, Dave Cummings, Jeremiah Currier, Yunxing Dai, Cory Decareaux, Thomas Degry, Noah Deutsch, Damien Deville, Arka Dhar, David Dohan, Steve Dowling, Sheila Dunning, Adrien Ecoffet, Atty Eleti, Tyna Eloundou, David Farhi, Liam Fedus, Niko Felix, Simón Posada Fishman, Juston Forte, Isabella Fulford, Leo Gao, Elie Georges, Christian Gibson, Vik Goel, Tarun Gogineni, Gabriel Goh, Rapha Gontijo-Lopes, Jonathan Gordon, Morgan Grafstein, Scott Gray, Ryan Greene, Joshua Gross, Shixiang Shane Gu, Yufei Guo, Chris Hallacy, Jesse Han, Jeff Harris, Yuchen He, Mike Heaton, Johannes Heidecke, Chris Hesse, Alan Hickey, Wade Hickey, Peter Hoeschele, Brandon Houghton, Kenny Hsu, Shengli Hu, Xin Hu, Joost Huizinga, Shantanu Jain, Shawn Jain, Joanne Jang, Angela Jiang, Roger Jiang, Haozhun Jin, Denny Jin, Shino Jomoto, Billie Jonn, Heewoo Jun, Tomer Kaftan, Łukasz Kaiser, Ali Kamali, Ingmar Kanitscheider, Nitish Shirish Keskar, Tabarak Khan, Logan Kilpatrick, Jong Wook Kim, Christina Kim, Yongjik Kim, Jan Hendrik Kirchner, Jamie Kiros, Matt Knight, Daniel Kokotajlo, Łukasz Kondraciuk, Andrew Kondrich, Aris Konstantinidis, Kyle Kosic, Gretchen Krueger, Vishal Kuo, Michael Lampe, Ikai Lan, Teddy Lee, Jan Leike, Jade Leung, Daniel Levy, Chak Ming Li, Rachel Lim, Molly Lin, Stephanie Lin, Mateusz Litwin, Theresa Lopez, Ryan Lowe, Patricia Lue, Anna Makanju, Kim Malfacini, Sam Manning, Todor Markov, Yaniv Markovski, Bianca Martin, Katie Mayer, Andrew Mayne, Bob McGrew, Scott Mayer McKinney, Christine McLeavey, Paul McMillan, Jake McNeil, David Medina, Aalok Mehta, Jacob Menick, Luke Metz, Andrey Mishchenko, Pamela Mishkin, Vinnie Monaco, Evan Morikawa, Daniel Mossing, Tong Mu, Mira Murati, Oleg Murk, David Mély, Ashvin Nair, Reiichiro Nakano, Rameesh Nayak, Arvind Neelakantan, Richard Ngo, Hyeonwoo Noh, Long Ouyang, Cullen O’Keefe, Jakub Pachocki, Alex Paino, Joe Palermo, Ashley Pantuliano, Giambattista Parascandolo, Joel Parish, Emy Parparita, Alex Passos, Mikhail Pavlov, Andrew Peng, Adam Perelman, Filipe de Avila Belbute Peres, Michael Petrov, Henrique Ponde de Oliveira Pinto, Michael, Pokorny, Michelle Pokrass, Vitchyr H. Pong, Tolly Powell, Alethea Power, Boris Power, Elizabeth Proehl, Raul Puri, Alec Radford, Jack Rae, Aditya Ramesh, Cameron Raymond, Francis Real, Kendra Rimbach, Carl Ross, Bob Rotsted, Henri Roussez, Nick Ryder, Mario Saltarelli, Ted Sanders, Shibani Santurkar, Girish Sastry, Heather Schmidt, David Schnurr, John Schulman, Daniel Selman, Kyla Sheppard, Toki Sherbakov, Jessica Shieh, Sarah Shoker, Pranav Shyam, Szymon Sidor, Eric Sigler, Maddie Simens, Jordan Sitkin, Katarina Slama, Ian Sohl, Benjamin Sokolowsky,

- Yang Song, Natalie Staudacher, Felipe Petroski Such, Natalie Summers, Ilya Sutskever, Jie Tang, Nikolas Tezak, Madeleine B. Thompson, Phil Tillet, Amin Tootoonchian, Elizabeth Tseng, Preston Tuggle, Nick Turley, Jerry Tworek, Juan Felipe Cerón Uribe, Andrea Vallone, Arun Vijayvergiya, Chelsea Voss, Carroll Wainwright, Justin Jay Wang, Alvin Wang, Ben Wang, Jonathan Ward, Jason Wei, CJ Weinmann, Akila Welihinda, Peter Welinder, Jiayi Weng, Lilian Weng, Matt Wiethoff, Dave Willner, Clemens Winter, Samuel Wolrich, Hannah Wong, Lauren Workman, Sherwin Wu, Jeff Wu, Michael Wu, Kai Xiao, Tao Xu, Sarah Yoo, Kevin Yu, Qiming Yuan, Wojciech Zaremba, Rowan Zellers, Chong Zhang, Marvin Zhang, Shengjia Zhao, Tianhao Zheng, Juntang Zhuang, William Zhuk, and Barret Zoph. Gpt-4 technical report, 2024. URL <https://arxiv.org/abs/2303.08774>.
- Xichen Pan, Satya Narayan Shukla, Aashu Singh, Zhuokai Zhao, Shlok Kumar Mishra, Jialiang Wang, Zhiyang Xu, Jiuhai Chen, Kunpeng Li, Felix Juefei-Xu, Ji Hou, and Saining Xie. Transfer between modalities with metaqueries, 2025. URL <https://arxiv.org/abs/2504.06256>.
- Karl Pertsch, Kyle Stachowicz, Brian Ichter, Danny Driess, Suraj Nair, Quan Vuong, Oier Mees, Chelsea Finn, and Sergey Levine. Fast: Efficient action tokenization for vision-language-action models, 2025. URL <https://arxiv.org/abs/2501.09747>.
- Delin Qu, Haoming Song, Qizhi Chen, Zhaoqing Chen, Xianqiang Gao, Xinyi Ye, Qi Lv, Modi Shi, Guanghui Ren, Cheng Ruan, Maoqing Yao, Haoran Yang, Jiacheng Bao, Bin Zhao, and Dong Wang. Embodiedonevision: Interleaved vision-text-action pretraining for general robot control, 2025a. URL <https://arxiv.org/abs/2508.21112>.
- Delin Qu, Haoming Song, Qizhi Chen, Yuanqi Yao, Xinyi Ye, Yan Ding, Zhigang Wang, JiaYuan Gu, Bin Zhao, Dong Wang, and Xuelong Li. Spatialvla: Exploring spatial representations for visual-language-action model, 2025b. URL <https://arxiv.org/abs/2501.15830>.
- Prajit Ramachandran, Barret Zoph, and Quoc V. Le. Searching for activation functions, 2017. URL <https://arxiv.org/abs/1710.05941>.
- Hao Shi, Bin Xie, Yingfei Liu, Lin Sun, Fengrong Liu, Tiancai Wang, Erjin Zhou, Haoqiang Fan, Xiangyu Zhang, and Gao Huang. Memoryvla: Perceptual-cognitive memory in vision-language-action models for robotic manipulation, 2025. URL <https://arxiv.org/abs/2508.19236>.
- Haoming Song, Delin Qu, Yuanqi Yao, Qizhi Chen, Qi Lv, Yiwen Tang, Modi Shi, Guanghui Ren, Maoqing Yao, Bin Zhao, Dong Wang, and Xuelong Li. Hume: Introducing system-2 thinking in visual-language-action model, 2025. URL <https://arxiv.org/abs/2505.21432>.
- Jianlin Su, Yu Lu, Shengfeng Pan, Ahmed Murtadha, Bo Wen, and Yunfeng Liu. Roformer: Enhanced transformer with rotary position embedding, 2023. URL <https://arxiv.org/abs/2104.09864>.
- Gemini Robotics Team, Saminda Abeyruwan, Joshua Ainslie, Jean-Baptiste Alayrac, Montserrat Gonzalez Arenas, Travis Armstrong, Ashwin Balakrishna, Robert Baruch, Maria Bauza, Michiel Blokzijl, et al. Gemini robotics: Bringing ai into the physical world. *arXiv preprint arXiv:2503.20020*, 2025a.
- Gemma Team, Aishwarya Kamath, Johan Ferret, Shreya Pathak, Nino Vieillard, Ramona Merhej, Sarah Perrin, Tatiana Matejovicova, Alexandre Ramé, Morgane Riviére, Louis Rouillard, Thomas Mesnard, Geoffrey Cideron, Jean bastien Grill, Sabela Ramos, Edouard Yvinec, Michelle Casbon, Etienne Pot, Ivo Penchev, Gaël Liu, Francesco Visin, Kathleen Kenealy, Lucas Beyer, Xiaohai Zhai, Anton Tsitsulin, Robert Busa-Fekete, Alex Feng, Noveen Sachdeva, Benjamin Coleman, Yi Gao, Basil Mustafa, Iain Barr, Emilio Parisotto, David Tian, Matan Eyal, Colin Cherry, Jan-Thorsten Peter, Danila Sinopalnikov, Surya Bhupatiraju, Rishabh Agarwal, Mehran Kazemi, Dan Malkin, Ravin Kumar, David Vilar, Idan Brusilovsky, Jiaming Luo, Andreas Steiner, Abe Friesen, Abhanshu Sharma, Abheesht Sharma, Adi Mayrav Gilady, Adrian Goedeckemeyer, Alaa Saade, Alex Feng, Alexander Kolesnikov, Alexei Bendebury, Alvin Abdagic, Amit Vadi, András György, André Susano Pinto, Anil Das, Ankur Bapna, Antoine Miech, Antoine Yang, Antonia Paterson, Ashish Shenoy, Ayan Chakrabarti, Bilal Piot, Bo Wu, Bobak Shahriari, Bryce Petrin,

- Charlie Chen, Charline Le Lan, Christopher A. Choquette-Choo, CJ Carey, Cormac Brick, Daniel Deutsch, Danielle Eisenbud, Dee Cattle, Derek Cheng, Dimitris Paparas, Divyashree Shivakumar Sreepathihalli, Doug Reid, Dustin Tran, Dustin Zelle, Eric Noland, Erwin Huiyenga, Eugene Kharitonov, Frederick Liu, Gagik Amirkhanyan, Glenn Cameron, Hadi Hashemi, Hanna Klimczak-Plucińska, Harman Singh, Harsh Mehta, Harshal Tushar Lehri, Hussein Hazimeh, Ian Ballantyne, Idan Szpektor, Ivan Nardini, Jean Pouget-Abadie, Jetha Chan, Joe Stanton, John Wieting, Jonathan Lai, Jordi Orbay, Joseph Fernandez, Josh Newlan, Ju yeong Ji, Jyotinder Singh, Kat Black, Kathy Yu, Kevin Hui, Kiran Vodrahalli, Klaus Greff, Linhai Qiu, Marcella Valentine, Marina Coelho, Marvin Ritter, Matt Hoffman, Matthew Watson, Mayank Chaturvedi, Michael Moynihan, Min Ma, Nabila Babar, Natasha Noy, Nathan Byrd, Nick Roy, Nikola Momchev, Nilay Chauhan, Noveen Sachdeva, Oskar Bunyan, Pankil Botarda, Paul Caron, Paul Kishan Rubenstein, Phil Culliton, Philipp Schmid, Pier Giuseppe Sessa, Pingmei Xu, Piotr Stanczyk, Pouya Tafti, Rakesh Shivanna, Renjie Wu, Renke Pan, Reza Rokni, Rob Willoughby, Rohith Vallu, Ryan Mullins, Sammy Jerome, Sara Smoot, Sertan Girgin, Shariq Iqbal, Shashir Reddy, Shruti Sheth, Siim Pöder, Sijal Bhatnagar, Sindhu Raghuram Panyam, Sivan Eiger, Susan Zhang, Tianqi Liu, Trevor Yacovone, Tyler Liechty, Uday Kalra, Utku Evci, Vedant Misra, Vincent Roseberry, Vlad Feinberg, Vlad Kolesnikov, Woohyun Han, Woosuk Kwon, Xi Chen, Yinlam Chow, Yuvein Zhu, Zichuan Wei, Zoltan Egyed, Victor Cotruta, Minh Giang, Phoebe Kirk, Anand Rao, Kat Black, Nabila Babar, Jessica Lo, Erica Moreira, Luiz Gustavo Martins, Omar Sanseviero, Lucas Gonzalez, Zach Gleicher, Tris Warkentin, Vahab Mirrokni, Evan Senter, Eli Collins, Joelle Barral, Zoubin Ghahramani, Raia Hadsell, Yossi Matias, D. Sculley, Slav Petrov, Noah Fiedel, Noam Shazeer, Oriol Vinyals, Jeff Dean, Demis Hassabis, Koray Kavukcuoglu, Clement Farabet, Elena Buchatskaya, Jean-Baptiste Alayrac, Rohan Anil, Dmitry Lepikhin, Sebastian Borgeaud, Olivier Bachem, Armand Joulin, Alek Andreev, Cassidy Hardin, Robert Dadashi, and Léonard Hussenot. Gemma 3 technical report, 2025b. URL <https://arxiv.org/abs/2503.19786>.
- Keyu Tian, Yi Jiang, Zehuan Yuan, Bingyue Peng, and Liwei Wang. Visual autoregressive modeling: Scalable image generation via next-scale prediction. In A. Globerson, L. Mackey, D. Belgrave, A. Fan, U. Paquet, J. Tomczak, and C. Zhang (eds.), *Advances in Neural Information Processing Systems*, volume 37, pp. 84839–84865. Curran Associates, Inc., 2024a. URL https://proceedings.neurips.cc/paper_files/paper/2024/file/9a24e284b187f662681440ba15c416fb-Paper-Conference.pdf.
- Keyu Tian, Yi Jiang, Zehuan Yuan, Bingyue Peng, and Liwei Wang. Visual autoregressive modeling: Scalable image generation via next-scale prediction, 2024b. URL <https://arxiv.org/abs/2404.02905>.
- Yang Tian, Sizhe Yang, Jia Zeng, Ping Wang, Dahua Lin, Hao Dong, and Jiangmiao Pang. Predictive inverse dynamics models are scalable learners for robotic manipulation, 2024c. URL <https://arxiv.org/abs/2412.15109>.
- Xinlong Wang, Xiaosong Zhang, Zhengxiong Luo, Quan Sun, Yufeng Cui, Jinsheng Wang, Fan Zhang, Yueze Wang, Zhen Li, Qiying Yu, et al. Emu3: Next-token prediction is all you need. *arXiv preprint arXiv:2409.18869*, 2024.
- Yuqi Wang, Xinghang Li, Wenxuan Wang, Junbo Zhang, Yingyan Li, Yuntao Chen, Xinlong Wang, and Zhaoxiang Zhang. Unified vision-language-action model, 2025. URL <https://arxiv.org/abs/2506.19850>.
- Chengyue Wu, Xiaokang Chen, Zhiyu Wu, Yiyang Ma, Xingchao Liu, Zizheng Pan, Wen Liu, Zhenda Xie, Xingkai Yu, Chong Ruan, and Ping Luo. Janus: Decoupling visual encoding for unified multimodal understanding and generation, 2024. URL <https://arxiv.org/abs/2410.13848>.
- Jinheng Xie, Weijia Mao, Zechen Bai, David Junhao Zhang, Weihao Wang, Kevin Qinghong Lin, Yuchao Gu, Zhijie Chen, Zhenheng Yang, and Mike Zheng Shou. Show-o: One single transformer to unify multimodal understanding and generation, 2024. URL <https://arxiv.org/abs/2408.12528>.
- An Yang, Anfeng Li, Baosong Yang, Beichen Zhang, Binyuan Hui, Bo Zheng, Bowen Yu, Chang Gao, Chengen Huang, Chenxu Lv, Chujie Zheng, Dayiheng Liu, Fan Zhou, Fei Huang, Feng Hu,

- Hao Ge, Haoran Wei, Huan Lin, Jialong Tang, Jian Yang, Jianhong Tu, Jianwei Zhang, Jianxin Yang, Jiayi Yang, Jing Zhou, Jingren Zhou, Junyang Lin, Kai Dang, Keqin Bao, Kexin Yang, Le Yu, Lianghao Deng, Mei Li, Mingfeng Xue, Mingze Li, Pei Zhang, Peng Wang, Qin Zhu, Rui Men, Ruize Gao, Shixuan Liu, Shuang Luo, Tianhao Li, Tianyi Tang, Wenbiao Yin, Xingzhang Ren, Xinyu Wang, Xinyu Zhang, Xuancheng Ren, Yang Fan, Yang Su, Yichang Zhang, Yinger Zhang, Yu Wan, Yuqiong Liu, Zekun Wang, Zeyu Cui, Zhenru Zhang, Zhipeng Zhou, and Zihan Qiu. Qwen3 technical report, 2025a. URL <https://arxiv.org/abs/2505.09388>.
- Shuai Yang, Hao Li, Yilun Chen, Bin Wang, Yang Tian, Tai Wang, Hanqing Wang, Feng Zhao, Yiyi Liao, and Jiangmiao Pang. Instructvla: Vision-language-action instruction tuning from understanding to manipulation, 2025b. URL <https://arxiv.org/abs/2507.17520>.
- Xiaohua Zhai, Basil Mustafa, Alexander Kolesnikov, and Lucas Beyer. Sigmoid loss for language image pre-training, 2023. URL <https://arxiv.org/abs/2303.15343>.
- Biao Zhang and Rico Sennrich. Root mean square layer normalization, 2019. URL <https://arxiv.org/abs/1910.07467>.
- Wenyao Zhang, Hongsi Liu, Zekun Qi, Yunnan Wang, Xinqiang Yu, Jiazhao Zhang, Runpei Dong, Jiawei He, Fan Lu, He Wang, Zhizheng Zhang, Li Yi, Wenjun Zeng, and Xin Jin. Dreamvla: A vision-language-action model dreamed with comprehensive world knowledge, 2025a. URL <https://arxiv.org/abs/2507.04447>.
- Zijian Zhang, Kaiyuan Zheng, Zhaorun Chen, Joel Jang, Yi Li, Siwei Han, Chaoqi Wang, Mingyu Ding, Dieter Fox, and Huaxiu Yao. Grape: Generalizing robot policy via preference alignment, 2025b. URL <https://arxiv.org/abs/2411.19309>.
- Qingqing Zhao, Yao Lu, Moo Jin Kim, Zipeng Fu, Zhuoyang Zhang, Yecheng Wu, Zhaoshuo Li, Qianli Ma, Song Han, Chelsea Finn, Ankur Handa, Ming-Yu Liu, Donglai Xiang, Gordon Wetstein, and Tsung-Yi Lin. Cot-vla: Visual chain-of-thought reasoning for vision-language-action models, 2025. URL <https://arxiv.org/abs/2503.22020>.
- Tony Z Zhao, Vikash Kumar, Sergey Levine, and Chelsea Finn. Learning fine-grained bimanual manipulation with low-cost hardware. *arXiv preprint arXiv:2304.13705*, 2023.
- Zhide Zhong, Haodong Yan, Junfeng Li, Xiangchen Liu, Xin Gong, Wenxuan Song, Jiayi Chen, and Haoang Li. Flowvla: Thinking in motion with a visual chain of thought, 2025. URL <https://arxiv.org/abs/2508.18269>.
- Chunting Zhou, Lili Yu, Arun Babu, Kushal Tirumala, Michihiro Yasunaga, Leonid Shamis, Jacob Kahn, Xuezhe Ma, Luke Zettlemoyer, and Omer Levy. Transfusion: Predict the next token and diffuse images with one multi-modal model, 2024. URL <https://arxiv.org/abs/2408.11039>.
- Chuning Zhu, Raymond Yu, Siyuan Feng, Benjamin Burchfiel, Paarth Shah, and Abhishek Gupta. Unified world models: Coupling video and action diffusion for pretraining on large robotic datasets, 2025. URL <https://arxiv.org/abs/2504.02792>.

A DATASET DETAILS

Our training corpus combines large internet-scale robot datasets with curated in-house demonstrations, spanning multiple embodiments (Genie-G1, Franka, WidowX, Google Robot, ARX LIFT II), camera viewpoints (third-person and wrist/head), and frame rates (3–30 FPS). In total, the corpus comprises 330.9K trajectories and 73.8M frames (Tab. 7).

Training proceeds in three stages. Pretrain Stages I–II primarily leverage the internet datasets, i.e., Agibot-World (AgiBot-World-Contributors et al., 2025), OXE-Fractal (Collaboration et al., 2025), OXE-Bridge-v2 (Collaboration et al., 2025), and LIBERO (Liu et al., 2023a), to provide broad coverage of manipulation behaviors and visual dynamics. Post-train Stage III adapts the model to specific skills using a smaller but higher-quality set of in-house demonstrations collected across diverse tasks, e.g., handover, sweeping, sorting, kitchen activities, and long-horizon manipulation, with Genie-G1, Franka, and ARX LIFT II.

Dataset	Source	Stage	Embodiment	Camera Views	FPS	# Trajs	# Frames
Agibot-World	Internet	I + II	Genie-G1	head + left/right wrist	30	187K	66.4M
LIBERO	Internet	I + II + III	Franka	3rd + wrist	20	1.7K	0.3M
OXE-Bridge-v2	Internet	I + II + III	WidowX	3rd	5	53.2K	1.9M
OXE-Fractal	Internet	I + II	Google Robot	3rd	3	87.2K	3.8M
Pen	In-house	III	Genie-G1	head + left/right wrist	30	152	78.1K
Flower	In-house	III	Genie-G1	head + left/right wrist	30	199	132.8K
Chip	In-house	III	Genie-G1	head + left/right wrist	30	100	54.7K
Tea (Table)	In-house	III	Genie-G1	head + left/right wrist	30	197	103.3K
Tea (Shelf)	In-house	III	Genie-G1	head + left/right wrist	30	202	112.0K
Bread	In-house	III	Genie-G1	head + left/right wrist	30	214	117.8K
Handover	In-house	III	Genie-G1	head + left/right wrist	30	171	124.4K
Handover (R2H)	In-house	III	Genie-G1	head + left/right wrist	30	210	144.5K
Sweep	In-house	III	Franka	3rd + wrist	15	59	43.8K
Sort	In-house	III	Franka	3rd + wrist	15	99	68.2K
Dynamic-Kitchen	In-house	III	ARX LIFT II	head + left/right wrist	30	48	57.6K
Long-horizon	In-house	III	ARX LIFT II	head + left/right wrist	30	129	347.3K
Total	-	-	-	-	-	330.9K	73.8M

Table 7: **Data Statistics.** Overview of internet-scale and in-house datasets used across different training stages. Internet datasets (top) provide large-scale pretraining data across varied robots and viewpoints, while curated in-house datasets (bottom) offer high-quality demonstrations for fine-tuning. In total, the combined corpus contains 330.9K trajectories and 73.8M frames.

B TRAINING DETAILS

Our model training is a three-stage process, with specific hyperparameters detailed in Tab. 8. Stage I focuses on learning general visual representations. It uses a large batch size of 1280 and a high learning rate of 3.0×10^{-4} over 512K training steps. In Stage II, we refine the model with a larger batch size of 2880 and a constant learning rate of 5.0×10^{-5} for 100K steps. This stage introduces action prediction, using a loss weight of 0.1:1 to balance generative and action losses. For Stage III, the model is finetuned on specific downstream tasks. All tasks in this stage share a smaller batch size of 128 and common settings for learning rate, and loss weight. However, the number of training steps (or epochs) and the Action Chunk Size are specifically adjusted for each task to account for differences in data volume and task difficulty, ensuring optimal performance across the board.

C REAL-WORLD TASK DETAILS

We evaluate our approach across multiple robotic platforms with tasks categorized by their core manipulation requirements and complexity levels. Our task suite spans from basic pick-and-place operations to complex long-horizon sequences, testing fundamental capabilities including precision manipulation, dual-arm coordination, human-robot interaction, and dynamic adaptation.

Hyperparameters	Stage I	Stage II	Stage III					
			LIBERO	Simpler	Genie-1	Franka	Dynamic	Long-horizon
Batch Size	1280	2880	128	128	128	128	128	128
Learning Rate	3.0×10^{-4}	5.0×10^{-5}	5.0×10^{-5}	5.0×10^{-5}	5.0×10^{-5}	5.0×10^{-5}	5.0×10^{-5}	5.0×10^{-5}
LR Scheduler	Cosine	Constant	Cosine	Cosine	Cosine	Cosine	Cosine	Cosine
Loss Weight (Gen:Act)	-	0.1:1	0.1:1	0.1:1	0.1:1	0.1:1	0.1:1	0.1:1
Training Epochs	-	-	-	10	40	40	40	60
Training Steps	512K	100K	100K	-	-	-	-	-
Und Resolution	224×224	224×224	224×224	224×224	224×224	224×224	224×224	224×224
Gen Resolution	256×256	256×256	256×256	256×256	256×256	256×256	256×256	256×256
# Num Predicted Scales	10	4	4	4	4	4	4	4
Action Chunk Size	-	30	4	8	50	50	50	50
Denoise Steps	-	-	10	10	10	10	10	10

Table 8: **Training recipe of \mathcal{F}_1 .** Due to significant differences in the number of demonstrations and task difficulty across downstream tasks, the settings for Stage III are not uniform.

C.1 BASIC PICK-AND-PLACE MANIPULATION

This category covers fundamental grasping and placement tasks involving everyday household objects. Representative instructions include: “Put the pen from the table into the pen holder”, “Pick up a bag of chips and place it into the basket”, and “Pick up a bottle of black tea and place it into the shopping cart”. The main challenges arise from the diverse physical properties of the objects, ranging from rigid items such as pens, to smooth packages like bags of chips, and deformable object such as plastic bottles, while also requiring consistent placement accuracy across target receptacles with varying constraints.

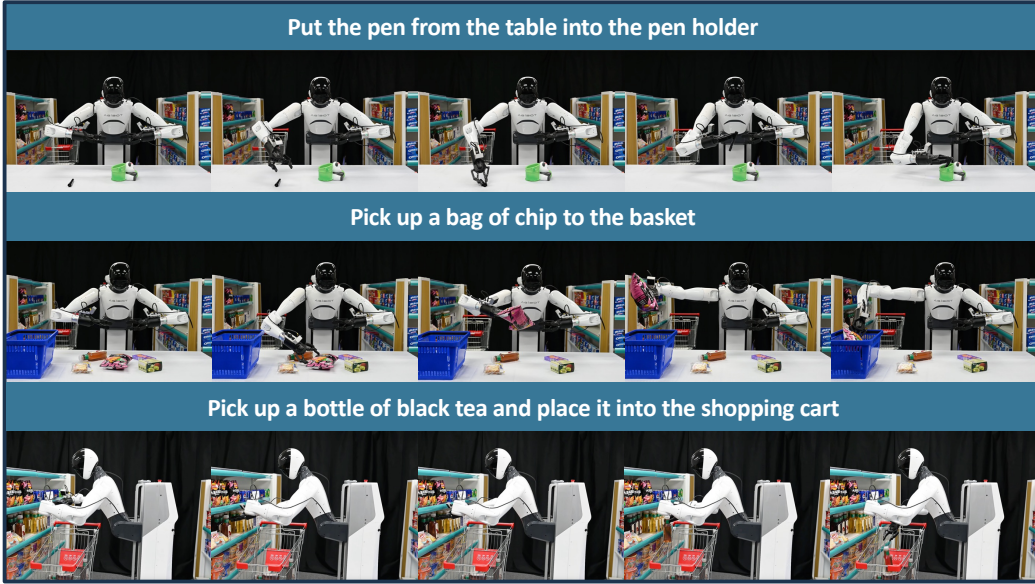


Figure 11: **Basic Pick-and-Place Manipulation.** Examples of fundamental grasping and placement tasks across different object types and target containers.

C.2 FINE-GRAINED PRECISION MANIPULATION

This category evaluates the limits of robotic fine motor control through tasks demanding high precision and delicate handling. A representative example, “Pick up the flower and insert it into the vase”, specifically assesses fine-grained grasping and placement under tightly constrained conditions. The challenge arises from the flower’s thin stem, which requires precise gripping to prevent damage, combined with the vase’s narrow opening, which demands accurate placement.



Figure 12: **Fine-Grained Precision Manipulation.** The robot is instructed to pick up the flower and insert it into the vase, which requires the precise control for handling delicate objects with narrow target constraints.

C.3 DUAL-ARM COORDINATION AND HUMAN-ROBOT INTERACTION

Bimanual manipulation tasks evaluate coordinated control of both robotic arms, focusing on spatial-temporal synchronization and inter-arm object transfer capabilities. The primary task in this category involves the instruction “Pick a bag of bread with the left arm, then handover, finally put it into the basket”, and “Pick a bottle of black tea and hand over to the person”, which requires seamless coordination between arms throughout the manipulation sequence.

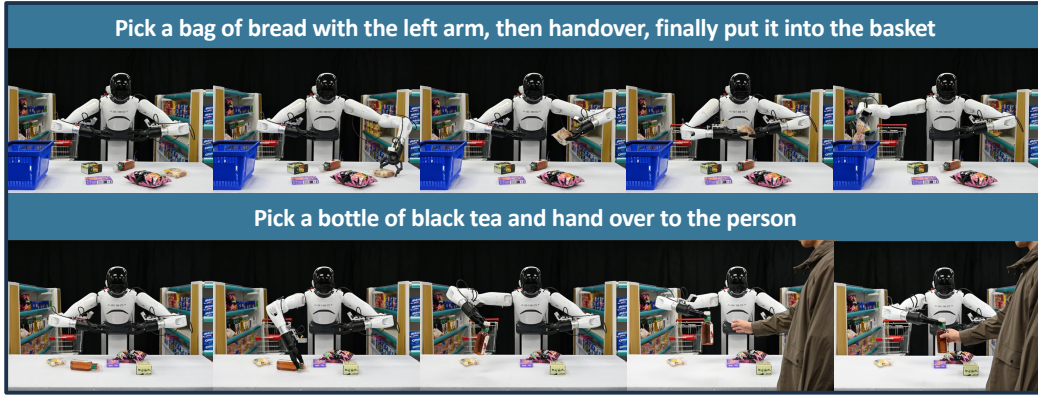


Figure 13: **Dual-Arm Coordination and Handover.** Examples of bimanual coordination and human-robot interaction tasks demonstrating inter-arm object transfer and collaborative handover capabilities.

C.4 DYNAMIC ENVIRONMENT ADAPTATION

Tasks in this category are performed within continuously changing environments, testing real-time tracking capabilities, and adaptive control under uncertainty. The instruction “Pickup the lettuce with the right hand and then the bread with the left hand” exemplifies the need for sophisticated trajectory prediction and real-time interception of moving targets. Additional challenges arise when robots must respond to unexpected dynamic events during task execution, such as objects falling or environmental conditions changing mid-operation.

C.5 LONG-HORIZON SEQUENTIAL MANIPULATION

Extended task sequences in this category demand comprehensive multi-step planning, coordinated tool use, and sustained task coherence across complex operation chains. As illustrated in Fig. 15, the key challenges include long-horizon planning over 10-step sequences with effective memory management, sequential coordination of multiple tools, handling objects with diverse physical properties—ranging from rigid and deformable to liquid materials—and dynamic replanning when unexpected events arise during execution.

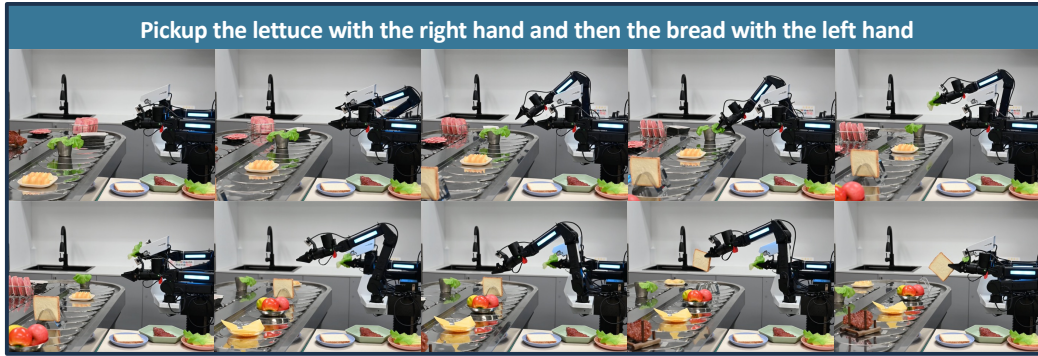


Figure 14: **Dynamic Environment Adaptation.** Example of real-time tracking and motion prediction capabilities in continuously changing environments. The robot successfully acquires specific food items from a moving belt.



Figure 15: **Long-Horizon Sequential Manipulation.** Example of extended multi-step task execution requiring comprehensive planning, tool usage, and task coherence maintenance.

D DEPLOY PLATFORM AND LATENCY ANALYSIS

All experiments are conducted on a workstation equipped with an Intel i9 CPU and an NVIDIA RTX 4090 GPU. All robots are connected to the host machine via wired Ethernet, thereby avoiding the additional transmission delays typically incurred in wireless communication. This setup ensures that the measured latency primarily reflects the computational overhead of the model itself. To provide a detailed view of system efficiency, we report the latency of each processing stage when the model takes three synchronized camera views as input. As shown in Tab. 9, the foresight generation and action decoding modules contribute the majority of the runtime, while image preprocessing and encoding remain relatively lightweight. Overall, the total inference time is approximately 235ms, which is sufficient for real-time deployment in embodied robotic scenarios.

Model Part	Inference Time
image process (e.g., resize)	18ms
temporal downsampling	28ms
image encoder	18ms
foresight generation	76ms
x10 action forward pass (flow)	95ms
total inference	235ms

Table 9: **Latency of \mathcal{F}_1 on the deployment platform (Intel i9 CPU + RTX 4090 GPU).** Robots are connected via wired Ethernet, so the reported numbers exclude wireless transmission delays.

E PROMPT TEMPLATE

Fig. 16 shows the full template used for evaluating foresight image quality with Qwen2.5-VL-32B-Instruct (Bai et al., 2025). The prompt explicitly specifies the input components (task instruction, four historical frames, the predicted next-step frame, and the ground-truth frame) and guides the evaluator to assign binary scores on three aspects: (i) scene consistency, (ii) object consistency, and (iii) task progress following. The model is instructed to output three numbers (0/1) together with a brief explanation.

Prompt Template

You are a visual sequence evaluation model for robot activity prediction.

You will be given the following inputs:

- A task instruction: "{task_name}"
- Four historical images (Image 1 to Image 4), representing a temporal sequence of the robot performing the task
- One generated image (Image 5), which is a predicted next step in the sequence
- One reference image (Image 5_GT), which is the ground-truth next image for comparison

Evaluate Image 5 based on the following three criteria:

- 1. Scene Consistency Score (0 or 1) :**
Does Image 5 maintain spatial and environmental consistency with Images 1–4? This includes:
 - Background layout and geometry should remain stable across the sequence
 - Lighting, colors, and textures must remain coherent
 - If Image 5 is **blurry, low-resolution, or lacks structural detail**, assign a score of 0
- 2. Object Consistency Score (0 or 1):**
Are key objects consistent in **presence, identity, appearance, and position** compared with Images 1–4?
 - Blurry, missing, deformed, or hallucinated objects should lead to a score of 0
 - The robot itself should also be treated as a key object
- 3. Task Progress Following Score (0 or 1):**
Based on the task instruction and the visual progression from Images 1–4, does Image 5 show a plausible and coherent next action?
Additionally, compare Image 5 to Image 5_GT:
 - If Image 5 significantly deviates from Image 5_GT in a way that hinders task progression, score 0

Your evaluation should be **STRICT**.

Return **exactly three numbers (0 or 1)** separated by spaces, followed by a **brief explanation**.

Output format (first line must be just the 3 numbers):

1 0 1, Reason: Image 5 maintains background structure, but the object being manipulated is blurred and appears in a different shape. However, the robot continues a plausible motion toward the goal based on the task instruction.

Important: First return three numbers, separated by spaces, then a newline, including any explanations and inferences, but without any additional text.

Figure 16: **Prompt Template for Future Observation Quality Evaluation.** We adopt a MLLM as evaluator, i.e., Qwen2.5-VL-32B-Instruct, and design a prompt template from three aspects to evaluate the quality of generated future observation: 1) Scene Consistency, 2) Object Consistency, and 3) Task Progress Following.